NASA Technical Paper 3167

1992

A Simplified Method for Thermal Analysis of a Cowl Leading Edge Subject to Intense Local Shock-Wave-Interference Heating

David M. McGowan,
Charles J. Camarda,
and Stephen J. Scotti
Langley Research Center
Hampton, Virginia

National Aeronautics and Space Administration
Office of Management
Scientific and Technical Information Program

Abstract

Type IV shock-wave-interference heating on a blunt body causes extremely intense heating over a very localized region of the body. This paper presents an analytical solution to a heat-transfer problem that approximates the shock-wave-interference heating of an engine cowl leading edge of the National Aero-Space Plane. The problem uses a simplified geometry to represent the leading edge. An analytical solution is developed that provides a means for approximating maximum temperature differences between the outer- and inner-surface temperatures of the leading edge. The solution is computationally efficient and, as a result, is well suited for conceptual and preliminary design or trade studies. Transient and steady-state analyses are conducted, and results obtained from the analytical solution are compared with results of two-dimensional thermal-finite-element analyses over a wide range of design parameters. Isotropic materials as well as laminated composite materials are studied. Results of parametric studies are presented to indicate the effects of the thickness of the cowl leading edge and the width of the region affected by the shock-wave-interference heating on the thermal response of the leading edge. Finally, a nondimensional temperature parameter is developed that is useful in evaluating the effects of several design parameters on the thermal response of the leading edge.

Introduction

One of the critical design problems for reusable air-breathing hypersonic vehicles, such as the National Aero-Space Plane (NASP), is caused by the severe shock-wave-interference heating that can occur on the leading edge of the engine cowl. This heating can occur when the oblique vehicle-nose bow shock wave or the oblique engine-inlet-ramp shock waves intersect the cowl-leading-edge bow shock wave (ref. 1). This shock-wave intersection is likely to occur because the oblique shock waves, which compress the airflow external to the engine, must be located close to the cowl leading edge to maximize mass capture at the engine inlet to achieve efficient engine performance. The effects of shock-wave-interference heating must be considered in the design of cowl-leading-edge concepts for hypersonic vehicles such as NASP because the intense local heating results in very high local temperatures, very high temperature differences through the cowl-leading-edge thickness, and very high thermal stresses in the leading edge (refs. 2 to 4).

Recent experimental results for dynamic pressures lower than those expected in hypersonic flight (refs. 5 to 7) have been compared with computational-fluid-dynamics (CFD) predictions (refs. 2 and 8 to 10). The CFD predictions include the calculation of structural temperatures and thermal stresses with a finite-element method to solve a nonlinear, coupled system of aerothermal-structural equations (ref. 2). Results of this analysis substantiate the potential severity of the thermal stresses in the cowl leading edge. However, a CFD analysis is computationally expensive and not well suited for conceptual and preliminary design studies. Simpler, faster solution procedures are needed for the preliminary design of thermal-structural concepts for the engine cowl leading edges of future hypersonic vehicles.

This paper presents an analytical solution to a transient, linear heat-transfer problem that simulates two-dimensional (2-D) heat conduction in the skin of an engine cowl leading edge subjected to intense local surface heating representative of Type IV shock-wave-interference heating. The heat-transfer problem uses a simplified geometry to represent the leading edge, and the analytical solution to this problem provides a means for approximating the maximum temperatures in the skin of the cowl leading edge. Results obtained from this solution are compared with results of a finite-element analysis of the problem in which a more realistic cowl-leading-edge geometry is modeled. Analytical and finite-element solutions to a transient heat-transfer problem in which the region of intense heating sweeps across the cowl leading edge are used to determine the effect of the sweep speed of the heated region on the maximum temperature difference through the cowl-leading-edge thickness. Results obtained from analytical and finite-element solutions to a steady-state problem in which the region of intense heating remains stationary are also compared. Results of parametric studies are presented for various materials, including composites with graphite fibers that have a very high thermal conductivity along the length of the fibers. The parameters varied are the cowl-leading-edge thickness and the width of the region of intense heating. Finally, a nondimensional temperature parameter is developed that aids in the investigation of the effects of several design parameters on the maximum temperature difference in the cowl leading edge.

Symbols

A	cross-sectional area, in^2
A_n, B_n	coefficients used in analytical solution (see eqs. (A32) and (A33))
a_n, b_n	Fourier coefficients

c	square root of ratio of orthotropic thermal conductivities (see eq. (3))
c_p	specific heat at constant pressure, Btu/lb-°F
D, H	analytical solution parameters, in^{-1}
h	cowl-leading-edge thickness, in.
$\mathbf{i}$	unit vector
k	thermal conductivity, Btu/ft-hr-°F
L	length used in analytical solution (see eq. (3)), in.
M	Mach number
q	magnitude of external aerodynamic heating on cowl leading edge, Btu/ft^2-sec
q_o	magnitude of square heat pulse, Btu/ft^2-sec
q_{ref}	undisturbed stagnation point heat flux, Btu/ft^2-sec
r_1, r_2	inner and outer cowl-leading-edge radius, respectively, in.
T	temperature, °F
t	time, sec
V	square-heat-pulse sweep speed, in/sec
w	square-heat-pulse half-width, in.
X, Y	separation functions for analytical solution (see eq. (A7))
x, y	fixed Cartesian coordinate system for analytical solution
β	angular location from centerline of cowl, deg (see fig. 3)
ΔT	temperature difference, °F
θ	temperature difference, $T(\xi,\eta) - T_{\mathrm{in}}$,°F
λ_n	separation constants
ν	percent-fiber-volume content in composite materials
ξ, η	moving Cartesian coordinate system for analytical solution
ρ	density, lb/ft^3
Φ	nondimensional temperature parameter

Subscripts:

A	analytical
FE	finite element
in	inner surface
L, T	longitudinal and transverse direction, respectively
max	maximum
2	outer surface

Problem Definition

One of the critical issues for reusable air-breathing hypersonic vehicles, such as NASP, is the severity of the aerodynamic heating of the engine cowl leading edge. In addition to the undisturbed aerodynamic heating of the cowl leading edge that results from hypersonic flight, shock-wave-interference heating causes very high local increases in aerodynamic heating. This severe shock-wave-interference heating occurs when the oblique vehicle-nose bow shock wave or the oblique engine-inlet-ramp shock waves intersect the cowl-leading-edge bow shock wave, as shown in figure 1.

When this shock-wave intersection occurs, six types of interference patterns can develop that affect external aerodynamic heating at various interaction locations on the cowl (ref. 1). Of these types of patterns, the Type IV interference pattern produces the most severe heating because it results in a supersonic jet that impinges on the cowl leading edge. A schematic diagram of the Type IV interference pattern is shown in figure 2. The details of the flow in the supersonic jet are described in reference 6. If the supersonic jet impinges nearly normal to the cowl-leading-edge surface, it causes a localized jet stagnation region on the leading-edge surface, and the resulting aerodynamic heating may be more than 30 times greater than the undisturbed stagnation value (ref. 7).

A possible scenario for the formation of a Type IV shock-wave-interference pattern on an engine cowl leading edge of a hypersonic vehicle is described in reference 2 and is illustrated in figure 3. The hypersonic vehicle is assumed to be accelerating at Mach 16 with an oblique vehicle-nose bow shock wave initially located outboard of a scramjet engine (fig. 3(a)). In figure 3(a), β is a measure of the angle (in degrees) from the centerline of the leading edge and is positive in the counterclockwise direction. As the vehicle accelerates through Mach 16, the oblique vehicle-nose bow shock wave sweeps across the cowl leading edge

and intersects the cowl-leading-edge bow shock wave; thus, local aerodynamic heating is increased from the effects of shock-wave-interference heating. At a certain intersecting location, the Type IV interference pattern is formed and a supersonic jet impinges on the leading edge (fig. 3(b)). The jet then dissipates as the vehicle-nose bow shock wave moves farther inboard (fig. 3(c)) and a less severe Type III shear-layer-interference pattern is formed.

The change in the local heating distribution caused by the different shock-wave-interference patterns is illustrated in figure 3(d). In the figure, q is the magnitude of the external aerodynamic heating on the cowl leading edge and t is the time at which the magnitude of the heating is measured. The dashed lines are instantaneous heat rate distributions, and the solid bell-shaped curve indicates the envelope of the heat rate distribution that is assumed in reference 2. The maximum value q_o at approximately $\beta = -22^\circ$ (at $t = 0.14$ sec) corresponds to the Type IV shock-wave-interference heating. Such severe local heating can cause very high outer-surface temperatures, very high temperature differences through the cowl-leading-edge thickness, and very high thermal stresses near the shock-wave impingement point on the leading edge. This shock-wave-interference heating complicates the thermal and structural analysis of the cowl leading edge because an accurate calculation of temperatures through the cowl-leading-edge thickness can require an integrated fluid-thermal-structural analysis (ref. 2). An integrated analysis may be required because of the coupling between the external fluid and thermal analyses. A simpler method for obtaining an approximate solution of temperatures within the skin of the cowl leading edge is desirable for use in preliminary design studies.

In the present paper, the shock-wave-interference heating problem is assumed to be two-dimensional in a plane perpendicular to the spanwise direction (fig. 1). Other simplifying assumptions include a simplified geometry to represent the cowl leading edge, a square-heat-pulse representation of the supersonic-jet heating on the outer cowl surface, orthotropic temperature-independent material properties, a constant temperature on the internal cowl surface (T_{in}), and negligible surface radiation heat transfer. The simplified problem is solved through use of classic techniques as well as a finite-element analysis that models a more realistic cowl-leading-edge geometry.

In a previous experimental study of shock-wave-interference heating on a cylindrical leading edge, the width of the region heated by the shock-wave-interference heating (referred to herein as the jet width) was estimated to be one-twentieth of the diameter of the cylinder used in the experiment (ref. 3). However, this estimate was based on experimental results at Mach 6 and 8 and may not be representative of values for higher Mach numbers. Errors in predicting the jet width can cause large errors in calculations of the thermal response of the leading edge. The effect of changes in the jet width on the maximum temperature difference in the leading edge is therefore determined subsequently by a parametric study.

An experimentally determined heat-rate distribution on a cylinder subjected to Type IV shock-wave-interference heating is given in reference 2 and is shown in figure 4(a). In this figure, the ratio q/q_{ref} is equal to the magnitude of the Type IV shock-wave-interference heating normalized to the magnitude of the undisturbed stagnation point heat flux and β is the angular location on the leading edge. For the present study, this distribution is approximated by a uniform square heat pulse of constant width $2w$. For the transient problem (fig. 4(b)), the square heat pulse moves across the cowl leading edge at a constant speed V. For the steady-state problem (fig. 4(c)), the square heat pulse is stationary and centered at $\beta = 0^\circ$. Since shock-wave-interference heating dominates the thermal response in the cowl leading edge, it is studied independently from the undisturbed stagnation heating.

The baseline cowl-leading-edge geometry selected for study is shown in figure 5. The cowl consists of a wedge with a cylindrical nose having an inner radius of 0.1 in. and straight sections 2 in. long inclined at angles of $\pm 8^\circ$ to the horizontal. The unit vectors $\mathbf{i}_T$ and $\mathbf{i}_L$ shown in the figure represent the directions of the orthotropic thermal conductivities. The thermal conductivity in the transverse direction (radial direction as shown in fig. 5) is k_T, and the thermal conductivity in the longitudinal direction is k_L. The inner-surface temperature T_{in} is assumed to remain constant. The assumption of a constant inner-surface temperature is made as an approximation for a liquid-metal heat-pipe-cooled concept or for a convectively cooled concept using a coolant with a high heat-transfer coefficient. However, it is, in general, a nonconservative assumption for convectively cooled concepts.

Materials Investigated

Both metallic and composite materials are considered in this study. The metallic materials investigated are copper and Incoloy Alloy 909 (a superalloy

made by Inco Alloys International, Inc.). The properties used for these materials are given in table I(a). Copper and Incoloy 909 are used to represent upper and lower bounds, respectively, of thermal conductivity for useful candidate materials for NASP. It is assumed that results from the steady-state analysis for materials with thermal conductivities within this range will be bracketed by these upper and lower bounds.

The composite materials investigated in this study consist of laminates of copper and Incoloy 909 with 50-percent fiber-volume fraction of high-conductivity graphite, such as highly oriented pyrolytic graphite (HOPG), or carbon fiber, such as Thornel P-140 carbon fiber. The HOPG (properties shown in table I(a)) is not available as a fiber, but its material properties are used in this study as an upper bound to illustrate the maximum capability that might be achievable for high-thermal-conductivity graphite fibers (ref. 11). The Thornel P-140 carbon fiber (properties shown in table I(a)) is a commercially available, ultrahigh-modulus, pitch-based carbon fiber with high longitudinal thermal conductivity (about twice that of copper) and relatively low transverse conductivity (ref. 12). Material properties for the composites are calculated based on parallel and series conduction paths through the material and fiber (ref. 13). Longitudinal and transverse thermal conductivities are calculated from the following relationships:

$$k_L = \nu k_{F,L} + (1 - \nu)\, k_M \tag{1}$$

$$k_T = \frac{k_M k_{F,T}}{\left[(1 - \nu)\, k_{F,T} + \nu k_M\right]} \tag{2}$$

In equations (1) and (2), k_L and k_T are the longitudinal and transverse thermal conductivities of the composite material, respectively, $k_{F,L}$ and $k_{F,T}$ are the longitudinal and transverse conductivities of the fiber, respectively, k_M is the conductivity of the matrix, and ν is the percent-fiber-volume content of the composite material. Bulk composite densities and specific heats are calculated by averaging the values of the constituent materials. The material properties for the composite materials used in this study are given in table I(b). These properties are assumed to remain constant with temperature.

2-D Finite-Element Analysis

The finite-element analysis system used in this study is the Engineering Analysis Language (EAL, ref. 14). The thermal-analyzer portion of EAL (ref. 15) is used to perform the thermal-finite-element analyses. For nonlinear problems (i.e., those including surface radiation), the analyzer iterates on nodal temperatures using a modified Newton method until convergence of the temperatures is obtained. Thermal-finite-element models of both the transient and the steady-state problem were developed, and both of these models, as well as the assumed boundary conditions, are described subsequently.

Transient Finite-Element Analysis

The finite-element analysis of the transient problem is performed with an implicit, transient-response thermal analyzer entitled TRTB. This analyzer integrates in time using the Crank-Nicolson method, and it uses the modified Newton method to solve for nodal temperatures at each time step (ref. 15).

A detailed view of the cylindrical portion of the cowl-leading-edge thermal-finite-element model is shown in figure 6. The inner-surface temperature T_{in} is assumed to remain constant, and material properties are assumed to remain constant with temperature. Heat is rejected from the external surface by radiation to space; a surface emissivity of 0.8 is assumed. Adiabatic boundary conditions are assumed at the ends of the model, as indicated in figure 6. The wall thickness h is equal to the outer radius minus the inner radius $(r_2 - r_1)$, and the temperature difference of interest in this study ΔT_{max} is equal to the maximum outer-surface temperature minus T_{in}. The supersonic jet is approximated by a square heat pulse of width $2w$. This square heat pulse is assumed to sweep across the entire curved portion of the leading edge at a constant speed V for the transient problem. The initial condition is $T(t = 0) = T_{\text{in}}$. The model of the cowl leading edge has 2688 degrees of freedom and consists of 2544 quadrilateral conduction elements, 384 line heat source elements, and 424 line radiation elements.

The discretization of the model shown in figure 6 is very fine around the cylindrical portion of the cowl leading edge. This discretization is used for two reasons: (1) to accurately represent a moving supersonic jet for the transient cases and (2) to model accurately 2-D heat conduction from the narrow region heated by the square heat pulse. The outer arc length of each element in the cylindrical portion of the leading edge is selected to be $0.2w$. At time $t = 0$, the square heat pulse is located over the first 10 elements of the fine mesh on the lower surface of the model. Movement of the square heat pulse around the leading edge to simulate the surface effect

of the supersonic-jet heating is achieved by shifting the square heat pulse clockwise one element at each time step. The time step used is calculated by dividing the arc length of the outer surface of the leading edge by the number of elements in the leading edge and the sweep speed of the supersonic jet. The square heat pulse is assumed to have a constant magnitude, width, and speed as it traverses the entire curved portion of the leading edge.

As illustrated in figure 3(d), the assumption of a uniform square-heat-pulse speed and a uniform magnitude of the heating is conservative compared with the actual heating environment. The actual transient heating reaches a peak when a Type IV supersonic-jet impingement occurs normal to the surface and then decreases as the incident shock continues to move across the leading edge. In addition, the uniform speed used in the present study will only equal the actual supersonic-jet speed at the symmetry point of the cowl. At all other locations, the actual speed would be higher.

Steady-State Finite-Element Analysis

The finite-element analysis of the steady-state problem is performed with a steady-state thermal analyzer entitled SSTA. Nonlinear problems (e.g., those including surface radiation) are solved as previously discussed. For the steady-state analysis, only half of the model shown in figure 6 is used to take advantage of the physical and thermal symmetries. Symmetry conditions at a location of $\beta = 0°$ on the leading edge are imposed by an adiabatic wall condition. Additionally, for the steady-state case, the square heat pulse is assumed to remain stationary at a location of $\beta = 0°$. The width of this pulse is equal to w, and it is referred to herein as the square-heat-pulse half-width.

Analytical Solution of Simplified Problem

Transient Solution

The curved geometry of the cowl leading edge shown in figure 6 is approximated by the planar rectangular region shown in figure 7. Neglecting curvature when calculating heat conduction in a curved cylinder is considered adequate when the ratio of the cylinder wall thickness h to the inner radius of the cylinder r_1 is less than 0.1. For this study, r_1 remains constant at 0.1 in. Thus, wall thicknesses less than or equal to 0.01 in. are considered small, and a rectangular approximation of a curved leading edge is considered appropriate. For the purposes of evaluation, wall thicknesses up to 0.03 in. are used in the present paper. It is expected that neglecting curvature of the cowl leading edge will be less appropriate as the value of h increases and approaches 0.03 in. The supersonic-jet heating is represented by a local square heat pulse that moves along the upper surface of the rectangular region at a constant speed V. Therefore, the simplified model of the shock-wave-interference heating problem consists of the rectangular region heated on the surface $y = h$ by a moving square heat pulse of magnitude q_o and width $2w$.

A coordinate system (ξ, η) moves with the square heat pulse as described in the appendix. The rectangular region is subject to constant-temperature boundary conditions along the surfaces at $\xi = L$, $\xi = -L$, and $\eta = 0$. These boundary conditions are applied to simplify the solution of the problem; however, erroneous results may occur if $|L|$ is too small. Therefore, L is retained as a parameter in the solution so that appropriate conditions for it can be determined. Radiation heat transfer from the high-temperature gas of the supersonic jet to the cowl-leading-edge surface is neglected because, for a maximum cowl-leading-edge outer radius of 0.13 in., the radiation-heat-transfer contribution can be assumed to be a small portion of the total cowl-leading-edge heat load (ref. 16). Radiation leaving the upper surface of the rectangular region is also neglected.

An analytical solution to this problem is obtained that provides an approximation to the temperatures in the cowl leading edge as a function of several parameters: square-heat-pulse sweep speed V, cowl-leading-edge wall thickness h, square-heat-pulse half-width w, longitudinal thermal conductivity k_L, transverse thermal conductivity k_T, and external heating rate q_o.

The development of the transient analytical solution to the simplified problem is presented in the appendix. In the analysis of this problem, the effects of any initial temperature distribution are assumed to be negligible (refs. 17 and 18). The solution to this problem as presented in the appendix is a quasi-steady-state solution since it further assumes that the temperature distribution is constant within the reference frame attached to the moving square heat pulse. However, in the present paper, this solution is referred to as the transient analytical solution, since it represents a solution to the moving-square-heat-pulse problem. As shown in the appendix, the transient analytical solution in the moving coordinate system (ξ, η) is

$$\theta(\xi,\eta)=\frac{q_o\exp(-H\xi)}{Lk_Tc}\left(\sum_{n=2,4,\ldots}^{\infty}\left\{\frac{1}{\lambda_n\left[H^2+\left(n^2\pi^2/4L^2\right)\right]}\right.\right.$$
$$\times\left[H\left(2\sin\frac{n\pi w}{2L}\cosh Hw\right)\right.$$
$$\left.-\frac{n\pi}{2L}\left(2\cos\frac{n\pi w}{2L}\sinh Hw\right)\right]$$
$$\left.\times\left(\sin\frac{n\pi\xi}{2L}\frac{\sinh\lambda_n c\eta}{\cosh\lambda_n ch}\right)\right\}$$
$$+\sum_{n=1,3,\ldots}^{\infty}\left\{\frac{1}{\lambda_n\left[H^2+\left(n^2\pi^2/4L^2\right)\right]}\right.$$
$$\times\left[H\left(2\cos\frac{n\pi w}{2L}\sinh Hw\right)\right.$$
$$\left.+\frac{n\pi}{2L}\left(2\sin\frac{n\pi w}{2L}\cosh Hw\right)\right]$$
$$\left.\left.\times\left(\cos\frac{n\pi\xi}{2L}\frac{\sinh\lambda_n c\eta}{\cosh\lambda_n ch}\right)\right\}\right) \tag{3}$$

where

$$\theta(\xi,\eta)=T(\xi,\eta)-T_{\text{in}}=\Delta T$$
$$\xi=x-Vt$$
$$H=\frac{\rho Vc_p}{2k_L}$$
$$\lambda_n=\sqrt{H^2+\left(n^2\pi^2/4L^2\right)}$$
$$c^2=\frac{k_L}{k_T}$$

By evaluating this equation at $\xi=0$ and $\eta=h$, we may obtain a prediction of the maximum difference between the outer- and inner-surface temperatures. The solution evaluated at this point is

$$\theta(0,h)-\Delta T_{\max}$$
$$=\frac{q_o}{Lk_Tc}\left(\sum_{n=1,3,\ldots}^{\infty}\left\{\frac{1}{\lambda_n\left[H^2+\left(n^2\pi^2/4L^2\right)\right]}\right.\right.$$
$$\times\left[H\left(2\cos\frac{n\pi w}{2L}\sinh Hw\right)\right.$$
$$\left.\left.+\frac{n\pi}{2L}\left(2\sin\frac{n\pi w}{2L}\cosh Hw\right)\right](\tanh\lambda_n ch)\right\}\right) \tag{4}$$

The boundary conditions assumed at $\xi=\pm L$, the rectangular approximation of a curved region, and the neglect of surface radiation heat transfer may all affect the accuracy of the solution. However, as shown subsequently, a comparison between the finite-element and analytical solutions shows that the analytical solution is accurate for a wide range of parametric variables and material selections. This range includes potential NASP cowl-leading-edge geometries and materials.

Steady-State Solution

To obtain an analytical solution to the steady-state problem in which the square heat pulse is stationary, the square-heat-pulse sweep speed V is set equal to zero in the transient analytical solution (eq. (3)). The analytical solution then reduces to

$$\theta(\xi,\eta)=\frac{8Lq_o}{\pi^2ck_T}$$
$$\times\sum_{n=1,3,\ldots}^{\infty}\left[\frac{\sin(n\pi w/2L)\sinh(n\pi c\eta/2L)\cos(n\pi\xi/2L)}{n^2\cosh(n\pi ch/2L)}\right] \tag{5}$$

By evaluating this equation at $\xi=0$ and $\eta=h$, we may obtain a prediction of the maximum difference between the outer- and inner-surface temperatures for the steady-state case. The solution evaluated at this point is

$$\theta(0,h)=\Delta T_{\max}$$
$$=\frac{8Lq_o}{\pi^2ck_T}$$
$$\times\sum_{n=1,3,\ldots}^{\infty}\left[\frac{\sin(n\pi w/2L)\tanh(n\pi ch/2L)}{n^2}\right] \tag{6}$$

Results and Discussion

In the present paper, the analytical solutions to the shock-wave-interference heating problem are compared with the finite-element solutions for both the transient and steady-state problems. The comparisons show the applicability of the analytical solutions over a wide range of the following parameters: square-heat-pulse sweep speed, cowl-leading-edge thickness, square-heat-pulse width, material orthotropic thermal conductivities, and magnitude of the shock-wave-interference heating. Parametric studies using the steady-state analytical solution are then conducted to investigate more closely the effects of changes in the cowl-leading-edge thickness and square-heat-pulse width on the maximum temperature differences. Finally, a nondimensional temperature parameter Φ is derived from the steady-state solution. This parameter is useful in evaluating the effects of all the aforementioned parameters on the maximum temperature difference.

Transient Finite-Element and Analytical Results

The effect of changes in the square-heat-pulse sweep speed on the maximum differences between the outer- and inner-surface temperatures is investigated with the transient finite-element analysis and the transient analytical solution (eq. (4)). Maximum temperature differences ΔT_{max} are calculated for a 0.01-in.-wide square heat pulse with a magnitude of 50 000 Btu/ft^2-sec sweeping across a 0.02-in.-thick cowl leading edge at uniform speeds ranging from 0 to 20.0 in/sec. (See table II.) The values of ΔT_{max} through the cowl-leading-edge thickness are calculated for a constant inner-surface temperature of 0°F, and they are shown as a function of square-heat-pulse sweep speed in figures 8 and 9. Results for copper, P-140/copper, and HOPG/copper are shown in figure 8, and results for Incoloy 909, P-140/Incoloy 909, and HOPG/Incoloy 909 are shown in figure 9. In these figures and those that follow, the maximum temperatures shown may exceed the allowable temperatures for the materials indicated in some circumstances. However, for the purposes of discussion and evaluating the analytical solutions, these results are retained unless otherwise noted.

As shown in figures 8 and 9, the results from the analytical solution overpredict ΔT_{max} (compared with the results from the finite-element analysis) for all the materials and square-heat-pulse sweep speeds except for copper and Incoloy 909. The analytical and finite-element results agree for the copper, and for Incoloy 909 the analytical solution overpredicts ΔT_{max} at $V = 0$ in/sec and underpredicts ΔT_{max} at $V \geq 2$ in/sec. However, the analytical and finite-element solutions give the same trends and agree (for the worst case of Incoloy 909) to within 15 percent.

The range of square-heat-pulse sweep speeds shown in figures 8 and 9 spans the range of expected NASP shock-wave sweep speeds (0.2 in/sec being the current expected value). Within the speed range of 0 to 2 in/sec (10 times the expected square-heat-pulse sweep speed), only Incoloy 909 shows an appreciable decrease in ΔT_{max} for increasing speed. This decrease in ΔT_{max} occurs because a smaller square-heat-pulse residence time reduces the amount of heat input locally into the leading edge, and this reduction compensates for the poor ability of Incoloy 909 to conduct heat from the square-heat-pulse region. Within this speed range, the maximum cowl-leading-edge temperatures for all the other materials reach a constant value almost instantaneously, and this value is very close to the steady-state (zero-square-heat-pulse speed) predictions of ΔT_{max} shown in figures 8 and 9. Therefore, the remaining studies use the steady-state analytical solution to investigate all the materials except Incoloy 909.

Steady-State Finite-Element and Analytical Results

The steady-state analytical and finite-element solutions are compared to assess the accuracy of the analytical solution. The analytical solution is used in parametric studies to investigate the effects of changes in the cowl-leading-edge thickness h (with the inner radius held constant) and the square-heat-pulse half-width w on the values of ΔT_{max}.

Accuracy of the analytical solution. Predictions of ΔT_{max} obtained from the steady-state analytical solution and from the steady-state finite-element analysis are compared in figure 10 to assess the accuracy of the analytical solution. The data represent results obtained from the two solutions while the following parameters are varied: longitudinal and transverse thermal conductivities k_L and k_T, cowl-leading-edge thickness h with the inner radius held constant, square-heat-pulse half-width w, heating rate q_o, and internal operating temperature T_{in}. The variations in thermal conductivity are obtained by changing materials, and the ranges of parameter variations used are shown in table II.

Results from the finite-element analysis are plotted on the ordinate in figure 10, and results from the analytical solution are plotted on the abscissa. The dashed line represents a perfect correlation between the two solutions, and the actual correlation between the two solutions, represented by the symbols, deviates very little from this line. The maximum difference (with respect to the analytical results) between the values of ΔT_{max} obtained from the analytical and finite-element solutions is less than 10 percent. Therefore, based on the assumption that the finite-element solution gives an accurate representation of the temperature distribution, such a correlation between the analytical and finite-element results indicates that the analytical solution is effective in predicting the maximum temperature differences in the cowl leading edge for a wide range of parameters.

Effect of changes in the cowl-leading-edge thickness on maximum temperature differences. The steady-state analytical solution is used to study the effect of changes in the cowl-leading-edge thickness h on the values of ΔT_{max}. Results from this aspect of the study are presented in figure 11 for copper, P-140/copper, and HOPG/copper and in figure 12 for P-140/Incoloy 909 and HOPG/Incoloy 909. The values of ΔT_{max} through the cowl leading edge are divided by the magnitude of the heat flux q_o so

that any value of heat flux may be considered. The values of $\Delta T_{max}/q_o$ are shown in figures 11 and 12 as a function of the cowl-leading-edge thickness h. For the results shown in these figures, the square-heat-pulse half-width w is assumed to be constant at $w = 0.005$ in.

As expected, the values of $\Delta T_{max}/q_o$ increase as the cowl-leading-edge thickness increases because the length of the transverse conduction path increases. Furthermore, the slopes of the curves are steeper for leading-edge thicknesses from 0.0025 to 0.0075 in. compared with the slopes for larger thicknesses. This effect occurs because the heat conduction in the leading edge is nearly one-dimensional in the transverse direction when the leading-edge thickness is small. Therefore, the maximum temperature difference is more sensitive to changes in the thickness. As the leading-edge thickness increases, the slopes of the curves decrease because the heat conduction becomes two-dimensional.

The results shown in figures 11 and 12 may also be used to determine the maximum temperature differences for potential cowl concepts. For example, if the maximum allowable cowl-leading-edge thickness h is 0.005 in. for a copper leading edge subjected to $q_o = 50\,000$ Btu/ft^2-sec, the value of $\Delta T_{max}/q_o$ is equal to 1°F-in^2-sec/Btu. This value corresponds to a maximum temperature difference of approximately 347°F. (See fig. 11.)

The effects of two-dimensional heat conduction in the cowl leading edge are also illustrated in figures 11 and 12. The values of $\Delta T_{max}/q_o$ for P-140/copper and HOPG/copper are larger than those for copper, as shown in figure 11. This result occurs because the transverse thermal conductivities of the composites are low compared with the thermal conductivity of copper. (See table I.) Furthermore, the values of $\Delta T_{max}/q_o$ for the HOPG/copper are lower than those for P-140/copper because the HOPG/copper has a higher longitudinal thermal conductivity than the P-140/copper and has the same transverse thermal conductivity. Similarly, the values of $\Delta T_{max}/q_o$ for HOPG/Incoloy 909 are lower than those for P-140/Incoloy 909 because the longitudinal thermal conductivity of HOPG/Incoloy 909 is higher than that of P-140/Incoloy 909.

Effect of changes in the square-heat-pulse width on maximum temperature differences. The width of the surface region affected by the shock-wave-interference supersonic jet used in the present study (i.e., the square-heat-pulse width) is taken from experimental results at $M = 6$ and 8 (ref. 3), and it may not be representative of values for higher Mach numbers. Therefore, the effect of changes in the square-heat-pulse width on maximum temperature differences predicted by the analytical solution is studied.

Values of $\Delta T_{max}/q_o$ for copper and P-140/copper are shown in figure 13 as a function of the square-heat-pulse half-width w for three cowl-leading-edge thicknesses. Similar results for P-140/Incoloy 909 and HOPG/Incoloy 909 are shown in figure 14. The sensitivity of the values of $\Delta T_{max}/q_o$ to changes in the square-heat-pulse half-width is equal to the slope $d(\Delta T_{max}/q_o)/dw$ of the curves in these figures. The values of the slopes are given in the figures for the curves corresponding to a cowl-leading-edge thickness of 0.03 in., with the assumption that $w = 0.005$ in. As shown in figure 13, the slope of the curve for a copper leading edge is approximately equal to 260°F-in^2-sec/Btu-in. Thus, the value of $\Delta T_{max}/q_o$ changes 260°F-in^2-sec/Btu per 1-in. change in w. The effect of this sensitivity to changes in the square-heat-pulse half-width is illustrated in the following example. For a copper leading edge, if it is assumed that $w = 0.005$ in., $h = 0.03$ in., and $q_o = 50\,000$ Btu/ft^2-sec, a value of $\Delta T_{max}/q_o = 1.67$°F-in^2-sec/Btu ($\Delta T_{max} = 580$°F) is calculated with the steady-state analytical solution. However, if the actual value of w is 50 percent higher (i.e., $w = 0.0075$ in.), the value of $\Delta T_{max}/q_o$ increases to 2.32°F-in^2-sec/Btu ($\Delta T_{max} = 805$°F). This new value represents a 38-percent increase over the original value. Similarly, the sensitivity of the P-140/copper composite is approximately 1590°F-in^2-sec/Btu-in. Therefore, for the same conditions described previously, the value of $\Delta T_{max}/q_o$ would increase by 40 percent. These high sensitivities of the maximum temperature difference to changes in the square-heat-pulse width indicate that the width of the square heat pulse can have an important effect on the thermal response of the leading edge.

The effects of two-dimensional heat conduction discussed previously are illustrated in figures 13 and 14 as well. A large decrease in transverse thermal conductivity (as in the case of P-140/copper compared with copper) or longitudinal thermal conductivity (as in the case of P-140/Incoloy 909 compared with HOPG/Incoloy 909) increases the sensitivity of the maximum temperature differences to changes in square-heat-pulse width. Another trend illustrated in figures 13 and 14 is that the sensitivity of the maximum temperature difference to changes in the square-heat-pulse width increases as the cowl-leading-edge thickness increases. This increase in the sensitivity occurs because the length of the transverse conduction path increases.

Nondimensional Temperature Parameter

The steady-state analytical solution (eq. (6)) is rearranged to obtain a nondimensional temperature parameter Φ that, for $L/w = 80$ (see appendix), is given as

$$\Phi = \frac{\Delta T_{\max}}{wq_o/ck_T} = \frac{640}{\pi^2} \sum_{n=1,3,\ldots}^{\infty} \left[\frac{\sin(n\pi/160)\tanh(n\pi ch/160w)}{n^2} \right] \quad (7)$$

The only term that will affect the summation on the right-hand side of equation (7) is the ratio hc/w. Thus, only wq_o/ck_T and hc/w govern the values of $\Delta T_{\max}$. The dependence of Φ on hc/w is shown in figure 15. The values of Φ presented in the figure are the converged values of the infinite series on the right-hand side of equation (7). (See appendix for a discussion of convergence.) The maximum temperature difference $\Delta T_{\max}$ can be determined from figure 15 for a given set of parameters. For example, if $hc/w = 1$, Φ is approximately equal to 3.47. The value for $\Delta T_{\max}$ can then be determined by multiplying 3.47 by the value of wq_o/ck_T.

Concluding Remarks

An analytical solution to a heat-transfer problem that approximates the problem of shock-wave-interference heating of the engine cowl leading edge of the National Aero-Space Plane (NASP) has been presented. The problem uses a simplified geometry to represent the leading edge and represents the supersonic jet that is characteristic of Type IV shock-wave-interference heating as a square heat pulse. The analytical solution provides a means for approximating maximum temperature differences between the outer and inner surfaces of the leading edge. Results of transient and steady-state analyses from the analytical solution were compared with results of two-dimensional finite-element analyses over numerous combinations of the following design parameters: square-heat-pulse sweep speed V (which varied from 0 to 20.0 in/sec), cowl-leading-edge thickness h (which varied from 0.005 to 0.030 in.), square-heat-pulse width $2w$ (which varied from 0.01 to 0.03 in.), transverse (radial) thermal conductivity k_T (which varied from 7 to 226 Btu/ft-hr-°F), longitudinal (normal to transverse) thermal conductivity k_L (which varied from 9 to 690 Btu/ft-hr-°F), and heat flux q_o (which varied from 10 000 to 100 000 Btu/ft^2-sec).

Results obtained with the transient, finite-element, and analytical solutions for square-heat-pulse sweep speeds expected for the NASP vehicle indicated that most of the materials used in this study responded nearly instantaneously to the shock-wave-interference heating. Thus, steady-state predictions of maximum temperature difference $\Delta T_{\max}$ were very close to the transient results.

An assessment of the accuracy of the steady-state analytical solution indicated that the analytical solution predicted maximum temperature differences to within 10 percent of the finite-element results. Parametric studies using the steady-state analytical solution were also performed to investigate the effects of changes in the cowl-leading-edge thickness and square-heat-pulse width on the maximum temperature differences for two different groups of materials. The materials investigated included copper, Incoloy 909, and laminated composites of these materials consisting of 50-percent fiber-volume fraction of either highly oriented pyrolytic graphite (HOPG) or Thornel P-140 carbon fibers. Copper and Incoloy 909 were chosen for study to represent upper and lower bounds, respectively, for thermal conductivity of useful NASP vehicle candidate materials for the engine cowl leading edge.

Results of the parametric studies illustrated that maximum temperature differences through the thickness of the leading edge increased when the cowl-leading-edge thickness was increased. Furthermore, the rate of change of the maximum temperature difference with increasing leading-edge thickness was larger when $0.0025 < h < 0.0075$ in. than it was when $h > 0.0075$ in. These studies also illustrated the effects of two-dimensional heat conduction in the leading edge by showing that large decreases in either the transverse thermal conductivity or the longitudinal conductivity of the leading-edge material resulted in increased maximum temperature differences.

The value of $\Delta T_{\max}$ was very sensitive to changes in the width of the square heat pulse used to simulate the shock-wave-interference heating. In one case, a 50-percent increase in this width resulted in an approximately 40-percent increase in $\Delta T_{\max}$. Additionally, large decreases in either the transverse or the longitudinal thermal conductivity of the leading-edge material resulted in increased sensitivity. Thus, the sensitivity of maximum temperature differences to changes in the square-heat-pulse width was affected by the two-dimensional nature of the heat conduction in the leading edge. The sensitivity of maximum temperature differences to changes in the width of the

square heat pulse also increased as the cowl-leading-edge thickness increased.

Finally, a nondimensional temperature parameter was derived from the steady-state analytical solution. Use of this parameter makes it possible to quickly calculate maximum temperatures and temperature differences in the cowl leading edge for the range of parameters considered in the present study.

NASA Langley Research Center
Hampton, VA 23665-5225
January 24, 1992

Appendix

Development of the Transient Analytical Solution

The transient, Type IV shock-wave-interference heating of the engine cowl leading edge shown in figure 6 is approximated by the transient, linear, two-dimensional heat-conduction problem represented in figure 7. The geometry is approximated by a planar rectangular region heated on the surface $y = h$ by a square heat pulse of magnitude q_o and width $2w$ that moves at a constant speed V. This appendix presents the development of the analytical solution to this problem.

Derivation of Governing Equation

The governing heat-transfer equation for transient, two-dimensional heat conduction is given by

$$\rho c_p \frac{\partial T}{\partial t} = k_L \frac{\partial^2 T}{\partial x^2} + k_T \frac{\partial^2 T}{\partial y^2} \tag{A1}$$

where k_L and k_T are the material thermal conductivities in the x- and y-directions, respectively. A reference frame may be attached (as in refs. 17 and 18) to the moving square heat pulse by replacing x, y, and t with new coordinates ξ, η, and τ such that

$$\xi = x - Vt \qquad \eta = y \qquad \tau = t$$

If $T = T(\xi, \eta, \tau)$,

$$\frac{\partial T}{\partial t} = \frac{\partial T}{\partial \xi}\frac{\partial \xi}{\partial t} + \frac{\partial T}{\partial \eta}\frac{\partial \eta}{\partial t} + \frac{\partial T}{\partial \tau}\frac{\partial \tau}{\partial t} = -V\frac{\partial T}{\partial \xi} + \frac{\partial T}{\partial \tau}$$

and equation (A1) may be rewritten as

$$\rho c_p \frac{\partial T}{\partial \tau} - V\rho c_p \frac{\partial T}{\partial \xi} = k_L \frac{\partial^2 T}{\partial \xi^2} + k_T \frac{\partial^2 T}{\partial \eta^2} \tag{A2}$$

If it is assumed that the temperature transient due to an initial condition has sufficiently decayed to have a negligible effect at the time of interest, the temperature distribution may be considered to be steady in the moving reference frame. (See refs. 17 and 18.) Therefore, the derivative with respect to τ in equation (A2) is zero, and the following equation results:

$$-V\rho c_p \frac{\partial T}{\partial \xi} = k_L \frac{\partial^2 T}{\partial \xi^2} + k_T \frac{\partial^2 T}{\partial \eta^2} \tag{A3}$$

or

$$c^2 T_{\xi\xi} + F T_\xi + T_{\eta\eta} = 0 \tag{A4}$$

where

$$c^2 = \frac{k_L}{k_T}$$

$$F = \frac{V\rho c_p}{k_T}$$

Equation (A4) is the governing heat-transfer equation of the transient, linear heat-conduction problem shown in figure 7. This equation can be solved subject to the following boundary conditions:

$$T(-L, \eta, \tau) = T_{\text{in}}$$
$$T(L, \eta, \tau) = T_{\text{in}}$$
$$T(\xi, 0, \tau) = T_{\text{in}}$$

$$q(\xi) = k_T \left.\frac{\partial T}{\partial \eta}\right|_{\eta=h} = \begin{cases} q_o & (-w \le \xi \le w) \\ 0 & (|\xi| > w) \end{cases}$$

Solution Procedure

Equation (A4) is a partial differential equation that may be solved in several ways. One solution procedure is as follows.

A new temperature variable may first be introduced through the following substitution:

$$\theta(\xi, \eta) = T(\xi, \eta) - T_{\text{in}} \tag{A5}$$

where T_{in} is the internal-surface temperature (at $\eta = 0$) that remains constant. Substituting equation (A5) into equation (A4) yields

$$c^2 \theta_{\xi\xi} + F\theta_{\xi} + \theta_{\eta\eta} = 0 \tag{A6}$$

The corresponding boundary conditions are

$$\theta(-L, \eta, \tau) = 0$$
$$\theta(L, \eta, \tau) = 0$$
$$\theta(\xi, 0, \tau) = 0$$

$$q(\xi) = k_T \left.\frac{\partial \theta}{\partial \eta}\right|_{\eta=h} = \begin{cases} q_o & (-w \le \xi \le w) \\ 0 & (|\xi| > w) \end{cases}$$

Now, through use of the method of separation of variables (ref. 19), a solution is assumed in the form

$$\theta(\xi, \eta) = X(\xi)\, Y(\eta) \tag{A7}$$

where $X(\xi)$ and $Y(\eta)$ are separation functions. Substituting this expression for θ into equation (A6) yields the following two ordinary differential equations:

$$c^2 X_{\xi\xi} + F X_{\xi} + \lambda^2 c^2 X = 0 \tag{A8}$$

$$Y_{\eta\eta} - \lambda^2 c^2 Y = 0 \tag{A9}$$

where λ is a separation constant.

Equation (A8) may be solved by assuming the solution:

$$X(\xi) = \exp(D\xi) \tag{A10}$$

Substituting this assumed solution into equation (A8) yields the following equation:

$$D^2 + 2HD + \lambda^2 = 0 \tag{A11}$$

where

$$2H = \frac{F}{c^2} = \frac{\rho V c_p}{k_T c^2} = \frac{\rho V c_p}{k_L}$$

Solving for D yields

$$D = -H \pm \sqrt{H^2 - \lambda^2} \tag{A12}$$

Therefore, the solution to equation (A8) is

$$X(\xi) = A \exp\left[\left(-H + \sqrt{H^2 - \lambda^2}\right)\xi\right] + B \exp\left[\left(-H - \sqrt{H^2 - \lambda^2}\right)\xi\right] \tag{A13}$$

where A and B are constants. The boundary conditions $\theta(\xi = -L) = \theta(\xi = L) = 0$ may be used to determine λ. Applying these boundary conditions results in

$$A \exp\left[\left(-H + \sqrt{H^2 - \lambda^2}\right)(-L)\right] + B \exp\left[\left(-H - \sqrt{H^2 - \lambda^2}\right)(-L)\right] = 0 \tag{A14}$$

$$A \exp\left[\left(-H + \sqrt{H^2 - \lambda^2}\right)L\right] + B \exp\left[\left(-H - \sqrt{H^2 - \lambda^2}\right)L\right] = 0 \tag{A15}$$

To obtain a nontrivial solution, the determinant of the coefficients for A and B in equations (A14) and (A15) is set equal to zero, the result being a linear dependence of the two equations. The following equation, which is solved for λ, results:

$$\exp\left(-2L\sqrt{H^2 - \lambda^2}\right) - \exp\left(2L\sqrt{H^2 - \lambda^2}\right) = 0 \tag{A16}$$

If $|\lambda| < |H|$, then the only solution for λ is $\lambda = H$; therefore, no solution exists. If $|\lambda| > |H|$, then the exponent is imaginary and, with Euler's identity, equation (A16) may be expressed as

$$2i \sin 2L\sqrt{\lambda^2 - H^2} = 0$$

Solving for λ yields

$$\lambda_n^2 = \frac{n^2\pi^2}{4L^2} + H^2 \tag{A17}$$

Rewriting the expression for D yields

$$D = -H \pm \sqrt{H^2 - \lambda^2} = -H \pm \frac{n\pi}{2L}i$$

This expression may be substituted into either equation (A14) or equation (A15) since these two equations are linearly dependent. Substituting the expression for D into equation (A14) yields

$$A_n \exp\left[\left(-H + i\frac{n\pi}{2L}\right)L\right] + B_n \exp\left[\left(-H - i\frac{n\pi}{2L}\right)L\right] = 0 \tag{A18}$$

Only the ratio of B_n/A_n can be determined from equation (A18). Therefore, for $A_n = 1$, it can be shown that B_n is

$$B_n = -\exp(in\pi) = -\cos n\pi - i \sin n\pi$$

For $n = 2, 4, ..., \sin n\pi = 0$ and $\cos n\pi = 1$. Therefore, $B_n = -1 - i(0) = -1$, and it may be shown that

$$X_n(\xi) = \exp(-H\xi) \sin \frac{n\pi\xi}{2L} \qquad (n = 2, 4, ...) \tag{A19}$$

For $n = 1, 3, ..., \sin\ n\pi = 0$ and $\cos n\pi = -1$. Therefore, $B_n = 1 - i(0) = 1$, and it may be shown that

$$X_n(\xi) = \exp(-H\xi) \cos \frac{n\pi\xi}{2L} \qquad (n = 1, 3, ...) \tag{A20}$$

Thus, equations (A19) and (A20) represent the solution for equation (A8).

Equation (A9) may be solved with the assumption of a solution of the form

$$Y_n(\eta) = E_n \sinh \lambda_n c\eta + F_n \cosh \lambda_n c\eta \tag{A21}$$

where E_n and F_n are constant coefficients. With the boundary condition $Y(0) = 0$, it can be shown that $Y_n(\eta)$, the solution to equation (A9), is

$$Y_n(\eta) = E_n \sinh \lambda_n c\eta \qquad (n = 1, 2, ...) \tag{A22}$$

Finally, with the substitution of equations (A19), (A20), and (A22) into equation (A7), the temperature difference between the temperature at any point in the moving coordinate system and T_{in} is

$$\begin{aligned} \theta(\xi, \eta) &= T(\xi, \eta) - T_{\text{in}} \\ &= \exp(-H\xi) \left(\sum_{n=2,4,...}^{\infty} A_n \sin \frac{n\pi\xi}{2L} \sinh \lambda_n c\eta \right. \\ &\quad \left. + \sum_{n=1,3,...}^{\infty} B_n \cos \frac{n\pi\xi}{2L} \sinh \lambda_n c\eta \right) \end{aligned} \tag{A23}$$

The coefficients A_n and B_n may be evaluated with the nonhomogeneous boundary condition

$$q(\xi) = k_T \left. \frac{\partial\theta}{\partial\eta} \right|_{\eta=h} = \begin{cases} q_o & (-w \le \xi \le w) \\ 0 & (|\xi| > w) \end{cases}$$

where, at $\eta = h$,

$$\begin{aligned} \frac{\partial\theta}{\partial\eta} &= c \exp(-H\xi) \left(\sum_{n=2,4,...}^{\infty} A_n \lambda_n \sin \frac{n\pi\xi}{2L} \cosh \lambda_n ch \right. \\ &\quad \left. + \sum_{n=1,3,...}^{\infty} B_n \lambda_n \cos \frac{n\pi\xi}{2L} \cosh \lambda_n ch \right) \end{aligned} \tag{A24}$$

Therefore

$$\begin{aligned} q(\xi)\ \exp(H\xi) &= k_T c \left(\sum_{n=2,4,...}^{\infty} A_n \lambda_n \sin \frac{n\pi\xi}{2L} \cosh \lambda_n ch \right. \\ &\quad \left. + \sum_{n=1,3,...}^{\infty} B_n \lambda_n \cos \frac{n\pi\xi}{2L} \cosh \lambda_n ch \right) \end{aligned} \tag{A25}$$

Equation (A25) is an infinite Fourier series. To solve for A_n and B_n, the Fourier coefficients a_n and b_n must be determined.

The Fourier coefficients are defined as follows:

$$a_n = \frac{1}{L}\int_{-L}^{L} f(\xi)\cos\frac{n\pi\xi}{2L}\,d\xi \qquad (n = 1, 3, ...) \tag{A26}$$

$$b_n = \frac{1}{L}\int_{-L}^{L} f(\xi)\sin\frac{n\pi\xi}{2L}\,d\xi \qquad (n = 2, 4, ...) \tag{A27}$$

where

$$f(\xi) = q(\xi)\ \exp(H\xi) = \exp(H\xi)\begin{cases} q_o & (-w \le \xi \le w) \\ 0 & (|\xi| > w) \end{cases}$$

Also,

$$a_n = B_n k_T \lambda_n c \cosh \lambda_n ch \tag{A28}$$

$$b_n = A_n k_T \lambda_n c \cosh \lambda_n ch \tag{A29}$$

Therefore, by carrying out the integration indicated in equations (A26) and (A27), a_n and b_n may be shown to be

$$a_n = \frac{q_o}{L\left[H^2 + (n^2\pi^2/4L^2)\right]}\left\{H\left[\exp(Hw)\cos\frac{n\pi w}{2L} - \exp(-Hw)\cos\frac{-n\pi w}{2L}\right] + \frac{n\pi}{2L}\left[\exp(Hw)\sin\frac{n\pi w}{2L} - \exp(-Hw)\sin\frac{-n\pi w}{2L}\right]\right\} \qquad (n = 1, 3, ...) \tag{A30}$$

$$b_n = \frac{q_o}{L\left[H^2 + (n^2\pi^2/4L^2)\right]}\left\{H\left[\exp(Hw)\sin\frac{n\pi w}{2L} - \exp(-Hw)\sin\frac{-n\pi w}{2L}\right] - \frac{n\pi}{2L}\left[\exp(Hw)\cos\frac{n\pi w}{2L} - \exp(-Hw)\cos\frac{-n\pi w}{2L}\right]\right\} \qquad (n = 2, 4, ...) \tag{A31}$$

By substitution of equations (A30) and (A31) into equations (A28) and (A29) and simplification of the results, it can be shown that A_n and B_n are

$$A_n = \left\{\frac{q_o}{Lk_T c\lambda_n \cosh\lambda_n ch\left[H^2 + (n^2\pi^2/4L^2)\right]}\left[H\left(2\sin\frac{n\pi w}{2L}\cosh Hw\right) - \frac{n\pi}{2L}\left(2\cos\frac{n\pi w}{2L}\sinh Hw\right)\right]\right\} \qquad (n = 2, 4, ...) \tag{A32}$$

$$B_n = \left\{\frac{q_o}{Lk_T c\lambda_n \cosh\lambda_n ch\left[H^2 + (n^2\pi^2/4L^2)\right]}\left[H\left(2\cos\frac{n\pi w}{2L}\sinh Hw\right) + \frac{n\pi}{2L}\left(2\sin\frac{n\pi w}{2L}\cosh Hw\right)\right]\right\} \qquad (n = 1, 3, ...) \tag{A33}$$

Finally, substituting equations (A32) and (A33) into equation (A23) gives the temperature distribution in the moving coordinate system (ξ, η):

$$\theta(\xi,\eta) = \frac{q_o \exp(-H\xi)}{Lk_T c}\left(\sum_{n=2,4,\ldots}^{\infty}\left\{\frac{1}{\lambda_n\left[H^2+(n^2\pi^2/4L^2)\right]}\left[H\left(2\sin\frac{n\pi w}{2L}\cosh Hw\right)\right.\right.\right.$$
$$\left.\left. - \frac{n\pi}{2L}\left(2\cos\frac{n\pi w}{2L}\sinh Hw\right)\right]\left(\sin\frac{n\pi\xi}{2L}\frac{\sinh\lambda_n c\eta}{\cosh\lambda_n ch}\right)\right\}$$
$$+\sum_{n=1,3,\ldots}^{\infty}\left\{\frac{1}{\lambda_n\left[H^2+(n^2\pi^2/4L^2)\right]}\left[H\left(2\cos\frac{n\pi w}{2L}\sinh Hw\right)\right.\right.$$
$$\left.\left.\left. + \frac{n\pi}{2L}\left(2\sin\frac{n\pi w}{2L}\cosh Hw\right)\right]\left(\cos\frac{n\pi\xi}{2L}\frac{\sinh\lambda_n c\eta}{\cosh\lambda_n ch}\right)\right\}\right) \tag{A34}$$

where

$$\theta(\xi,\eta) = T(\xi,\eta) - T_{\text{in}} = \Delta T(\xi,\eta)$$

In the present study, the maximum temperature difference $\Delta T_{\max}$ is assumed to be located at $\xi = 0$ and $\eta = h$; however, it will actually shift to $\xi < 0$ as the speed of the square heat pulse increases. The transient solution evaluated at $\xi = 0$ and $\eta = h$ is

$$\theta(0,h) = \Delta T_{\max}$$
$$= \frac{q_o}{Lk_T c}\left(\sum_{n=1,3,\ldots}^{\infty}\left\{\frac{1}{\lambda_n\left[H^2+(n^2\pi^2/4L^2)\right]}\left[H\left(2\cos\frac{n\pi w}{2L}\sinh Hw\right)\right.\right.\right.$$
$$\left.\left.\left. + \frac{n\pi}{2L}\left(2\sin\frac{n\pi w}{2L}\cosh Hw\right)\right](\tanh\lambda_n ch)\right\}\right) \tag{A35}$$

A steady-state form of the solution may be obtained by evaluating equation (A35) at $V = 0$. If this is done, the resulting equation for $\Delta T_{\max}$ is

$$\theta(0,h) = \Delta T_{\max} = \frac{8Lq_o}{\pi^2 ck_T}\sum_{n=1,3,\ldots}^{\infty}\left[\frac{\sin(n\pi w/2L)\tanh(n\pi ch/2L)}{n^2}\right] \tag{A36}$$

Convergence of the Analytical Solution

Since the transient and steady-state forms of the analytical solution (eqs. (A35) and (A36), respectively) are infinite series solutions, a convergence study was conducted to determine the number of terms necessary for an accurate solution. To simplify the convergence study, the steady-state analytical solution was used. However, the convergence criteria established as a result of the study were also applied to the transient analytical solution. The results of the convergence study are shown in figure 16. This figure shows the value of $\Delta T_{\max}$ as a function of the number of terms used in the solution. As shown in the figure, the analytical solution oscillates about a converged solution. The solution is considered to be converged when the percent difference between successive maximum and minimum values is less than 1 percent. The percent difference is calculated with respect to the latest maximum. The temperature difference $\Delta T_{\max}$ is then calculated to be the average of the most recent maximum and minimum values. For the case shown in figure 16, convergence occurs at 320 terms. However, the number of terms required for convergence varies from case to case.

Effect of the Assumed Boundary Conditions

To develop the analytical solution to the approximate problem, it is assumed that the temperatures along the edges $\xi = \pm L$ are equal to T_{in}. Therefore, the value of θ at these points is 0°F. This boundary condition may produce erroneous results if it is placed too close to the square-heat-pulse region because it may act as a heat sink and artificially reduce the maximum temperature difference between the outer and inner surfaces. Therefore, the effect of varying the value of L on the maximum temperature differences predicted by the analytical solution was investigated using the steady-state analytical solution. The results of the investigation are presented in figure 17, wherein the converged value of ΔT_{max} is shown as a function of L/w. (It is recognized that the temperatures shown in fig. 17 for the two composite materials exceed the maximum use temperatures for those materials; however, for the purpose of this discussion, the results are being retained.) As shown in the figure, the solution is unaffected by increases in L/w for $L/w > 80$. Thus, the value of L was set at $80w$ in all analyses.

Effect of Neglecting Radiation

The effects of radiation heat transfer leaving the outer surface of the cowl leading edge are neglected in the analytical solution. To investigate the validity of this assumption, several cases are investigated with the steady-state finite-element analysis (with P-140/Incoloy 909) used while T_{in} is varied from 0°F to 3000°F. The material P-140/Incoloy 909 was selected for this investigation because it has the lowest values of transverse and longitudinal thermal conductivities; therefore, it can be expected to have the highest surface temperatures for any given conditions. The results of the investigation are shown in figure 18. As shown in the figure, the maximum temperature difference decreases from approximately 4950°F to approximately 4600°F as T_{in} is varied from 0°F to 3000°F (a 7.1-percent decrease). The decreasing values of ΔT_{max} indicate that radiation heat transfer leaving the outer surface of the leading edge does become more important as T_{in} is increased. Since the increased internal temperatures cause the maximum outer-surface temperatures to increase, the amount of heat being radiated away from the leading edge increases. However, because typical values of T_{in} for a cowl-leading-edge structure should not exceed 2000°F, the effects of radiation heat transfer leaving the outer surface of the cowl leading edge are neglected in the present study.

References

1. Edney, Barry: *Anomalous Heat Transfer and Pressure Distributions on Blunt Bodies at Hypersonic Speeds in the Presence of an Impinging Shock.* FFA Rep. 115, Aeronautical Research Inst. of Sweden, 1968.

2. Dechaumphai, Pramote; Thornton, Earl A.; and Wieting, Allan R.: *Fluid-Thermal-Structural Study of Aerodynamically Heated Leading Edges.* NASA TM-100579, 1988.

3. Gladden, Herbert J.; Melis, Matthew E.; Mockler, Theodore T.; and Tong, Mike: *Thermal/Structural Analyses of Several Hydrogen-Cooled Leading-Edge Concepts for Hypersonic Flight Vehicles.* NASA TM 102391, 1990. (Available as AIAA-90-0053.)

4. Polesky, Sandra P.; Dechaumphai, Pramote; Glass, Christopher E.; and Pandey, Ajay K.: Three-Dimensional Thermal-Structural Analysis of a Swept Cowl Leading Edge Subjected to Skewed Shock-Shock Interference Heating. AIAA-90-1710, June 1990.

5. Wieting, Allan R.; and Holden, Michael S.: Experimental Shock-Wave Interference Heating on a Cylinder at Mach 6 and 8. *AIAA J.*, vol. 27, no. 11, Nov. 1989, pp. 1557–1565.

6. Wieting, Allan R.: *Experimental Study of Shock Wave Interference Heating on a Cylindrical Leading Edge.* NASA TM-100484, May, 1987.

7. Holden, M. S.; Wieting, A. R.; Moselle, J. R.; and Glass, C.: Studies of Aerothermal Loads Generated in Regions of Shock/Shock Interaction in Hypersonic Flow. AIAA-88-0477, Jan. 1988.

8. Stewart, James R.; Thareja, Rajiv R.; Wieting, Allan R.; and Morgan, Ken: Application of Finite Element and Remeshing Technique to Shock Interference on a Cylindrical Leading Edge. AIAA-88-0368, Jan. 1988.

9. Klopfer, G. H.; and Yee, H. C.: Viscous Hypersonic Shock-on-Shock Interaction on Blunt Cowl Lips. AIAA-88-0233, Jan. 1988.

10. Moon, Young J.; and Holt, Maurice: Interaction of an Oblique Shock Wave With Turbulent Hypersonic Blunt Body Flows. AIAA-89-0272, Jan. 1989.

11. Issi, J-P.: Thermal Transport in Intercalated Graphite. *Intercalated Graphite*, M. S. Dresselhaus, G. Dresselhaus, J. E. Fischer, and M. J. Moran, eds., *Volume 20 of Materials Research Society Symposia Proceedings*, Elsevier Science Publ. Co., Inc., c.1983, pp. 147–156.

12. Schulz, David A.: Advances in UHM Carbon Fibers: Production, Properties and Applications. *SAMPE J.*, vol. 23, Mar./Apr. 1987, pp. 27–31, 109.

13. Peterson, G. P.; and Fletcher, L. S.: A Review of Thermal Conductivity in Composite Materials. AIAA-87-1586, June 1987.

14. Whetstone, W. D.: *EISI-EAL Engineering Analysis Language Reference Manual—EISI-EAL System Level 2091.* Engineering Information Systems, Inc., July 1983.
Volume 1: General Rules and Utility Processors.
Volume 2: Structural Analysis—Primary Processors.

15. Marlowe, M. B.; Moore, R. A.; and Whetstone, W. D.: *SPAR Thermal Analysis Processors Reference Manual, System Level 16.* NASA CR-159162, 1979.

16. Anderson, John D., Jr.: *Hypersonic and High Temperature Gas Dynamics.* McGraw Hill, Inc., c.1989.

17. Rosenthal, D.: The Theory of Moving Sources of Heat and Its Application to Metal Treatments. *Trans. American Soc. Mech. Eng.*, vol. 68, 1946, pp. 849 866.

18. Rosenthal, Daniel: Mathematical Theory of Heat Distribution During Welding and Cutting. *J. American Weld. Soc.*, vol. 20, May 1941, pp. 220-s 234-s.

19. Boyce, William E.; and DiPrima, Richard C.: *Elementary Differential Equations and Boundary Value Problems, Third ed.*, John Wiley & Sons, Inc., c.1977.

Table I. Material Properties

(a) Constituent properties

Material	k_L, Btu/ft-hr-°F	k_T, Btu/ft-hr-°F	ρ, lb/in^3	c_p, Btu/lb-°F
Copper	226	226	0.322	0.10
Incoloy 909	9	9	.296	.11
P-140 carbon fiber	450	6	.050	.24
HOPG graphite	1156	6	.050	.24

(b) Composite properties (50-percent fiber-volume fraction)

Material	k_L, Btu/ft-hr-°F	k_T, Btu/ft-hr-°F	ρ, lb/in^3	c_p, Btu/lb-°F
P-140/copper	340	12	0.186	0.17
HOPG/copper	690	12	.186	.17
P-140/Incoloy 909	230	7	.173	.17
HOPG/Incoloy 909	583	7	.173	.17

Table II. Ranges of Parameter Variations

V, in/sec	0 to 20
q_o, Btu/ft^2-sec	10 000 to 100 000
k_L, Btu/ft-hr-°F	9 to 690
k_T, Btu/ft-hr-°F	7 to 226
k_L/k_T	1.0 to 83.3
$2w$, in.	0.01 to 0.03
h, in.	0.005 to 0.030

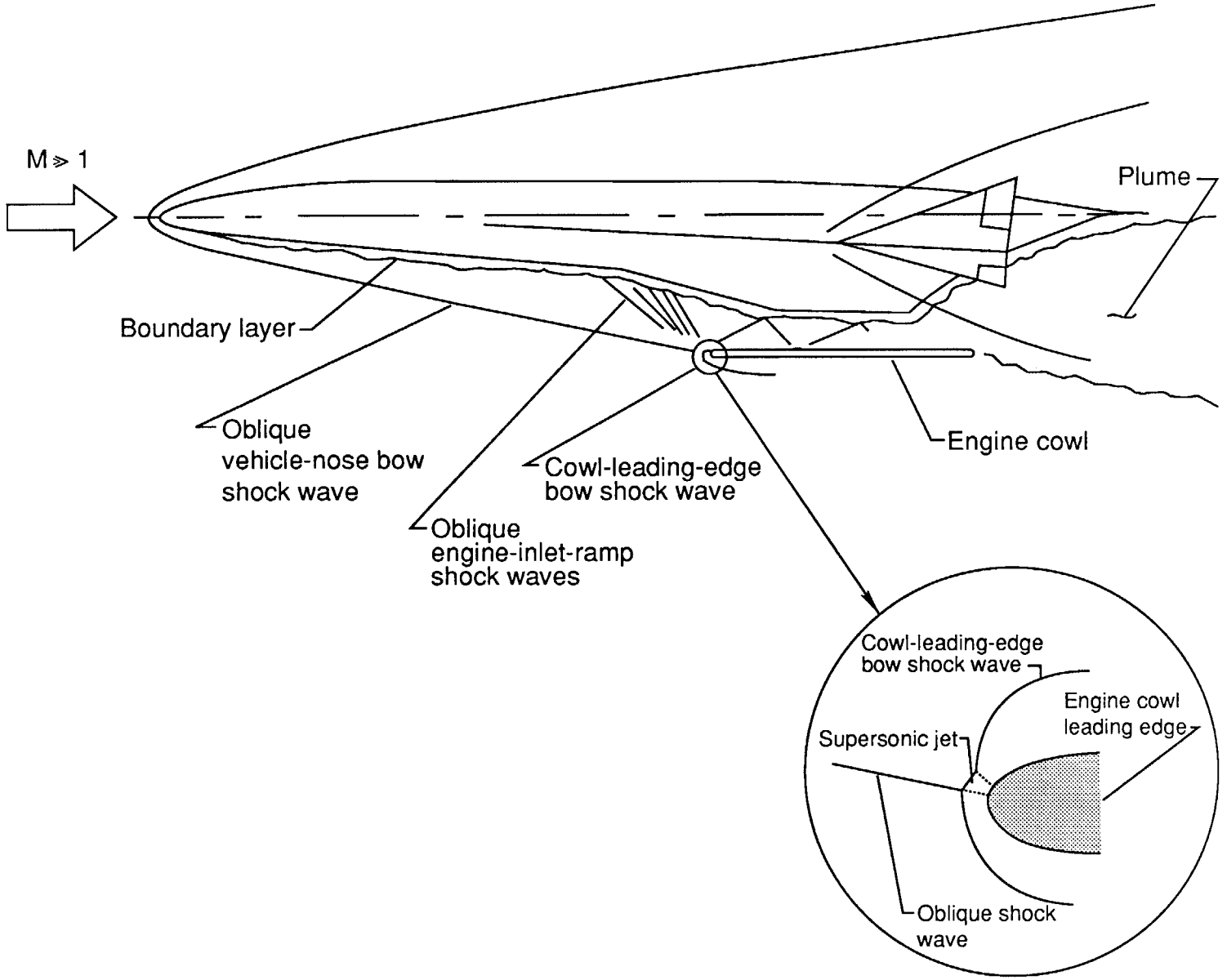

Figure 1. Expected Type IV shock-wave interference phenomenon occurring on engine cowl leading edge of reusable air-breathing hypersonic vehicle.

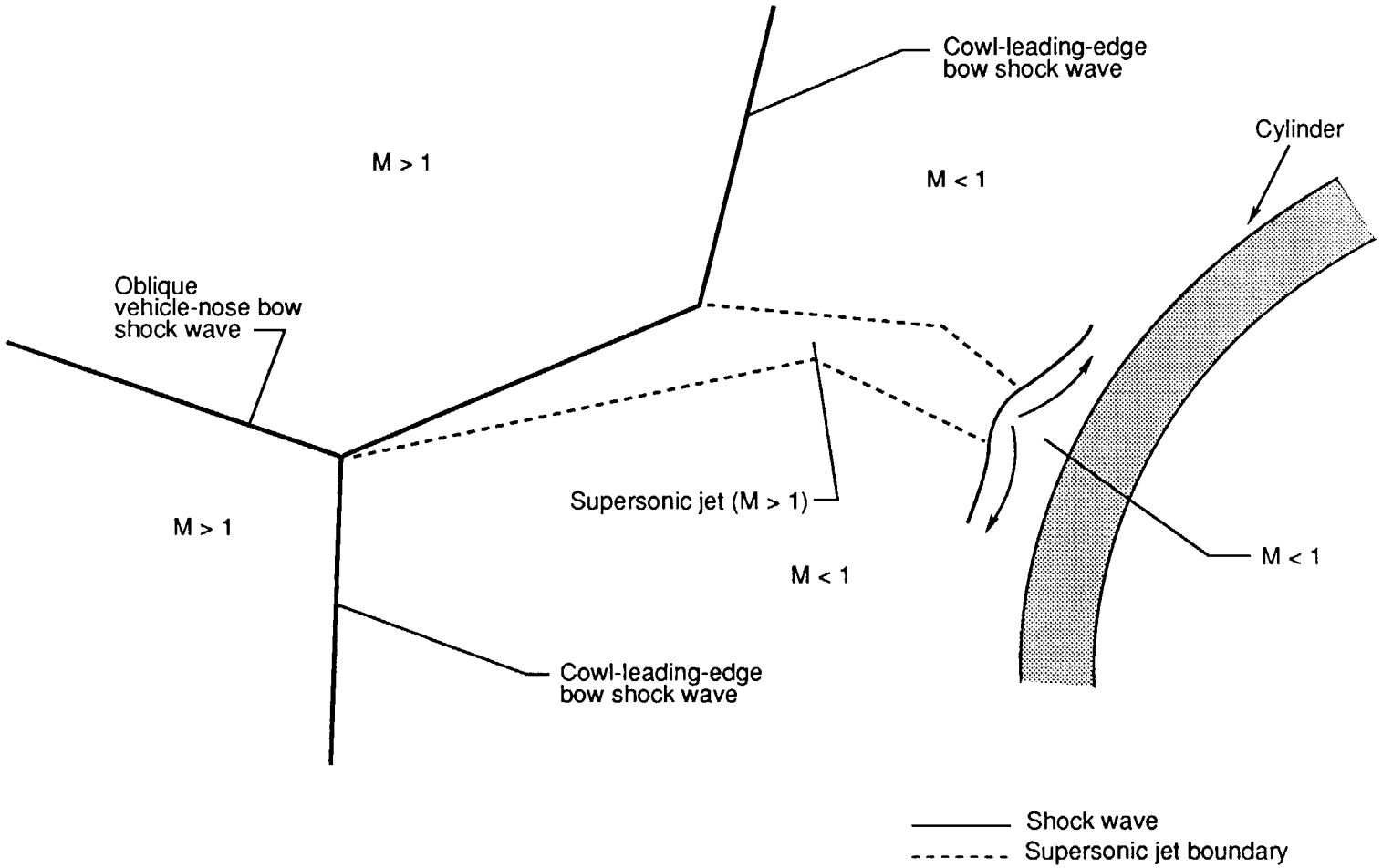

Figure 2. Schematic of Type IV shock-wave interference pattern (supersonic jet) impinging on a cylinder.

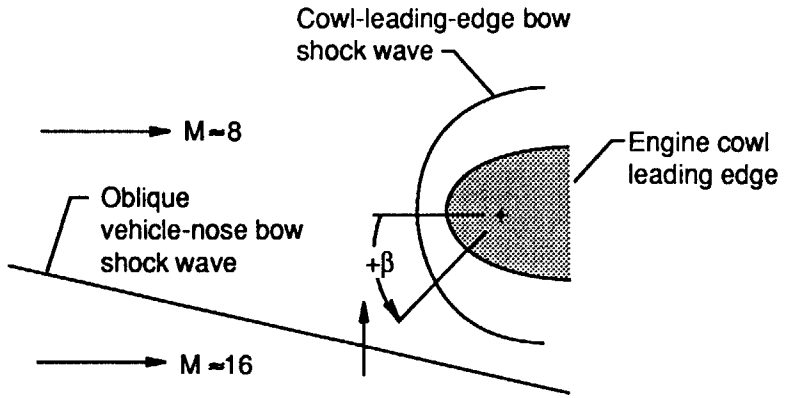

(a) Oblique vehicle-nose bow shock wave outboard of engine cowl leading edge. (Based on ref. 2.)

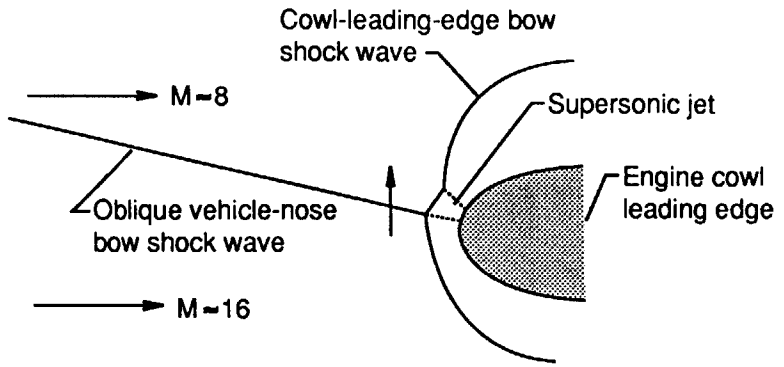

(b) Type IV shock-wave interference pattern formed as oblique vehicle-nose bow shock wave passes by engine cowl leading edge. (Based on ref. 2.)

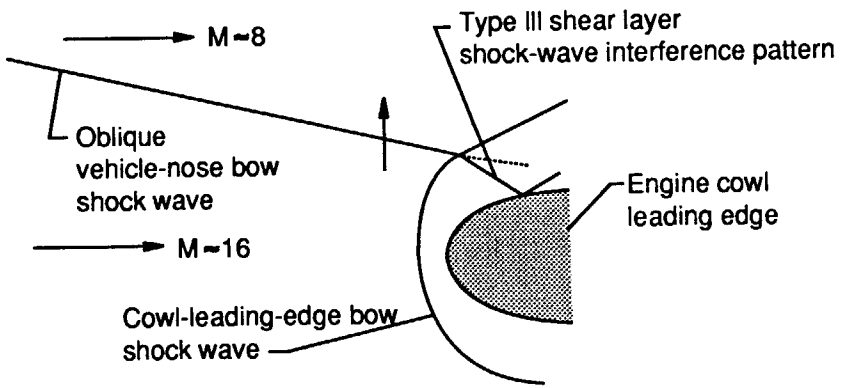

(c) Oblique vehicle-nose bow shock wave inboard of engine cowl leading edge. (Based on ref. 2.)

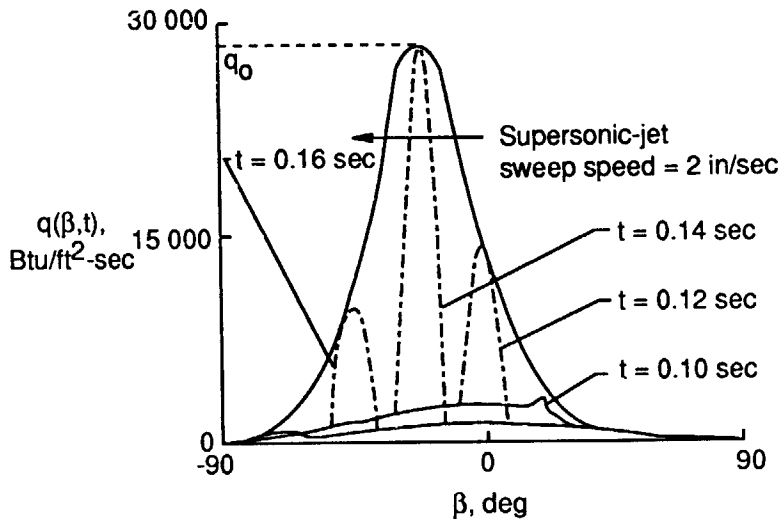

(d) Envelope of heat rate distribution on cowl leading edge. (From ref. 2.)

Figure 3. Development of Type IV shock-wave interference pattern on engine cowl leading edge.

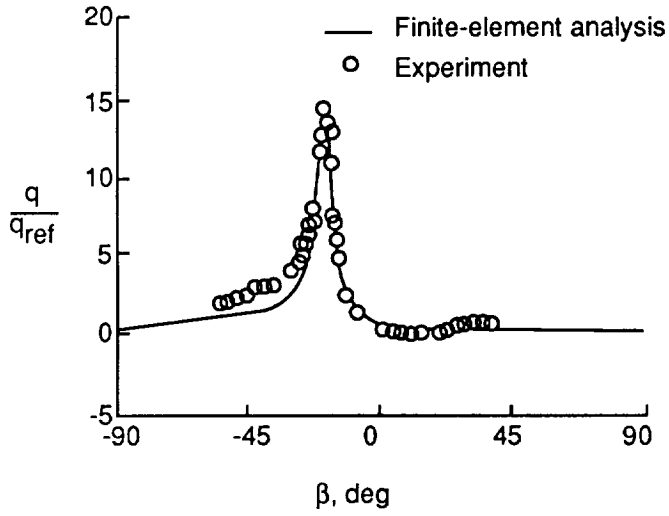

(a) Comparison of experimental and finite-element heating distributions. $M \approx 8$. (From ref. 2.)

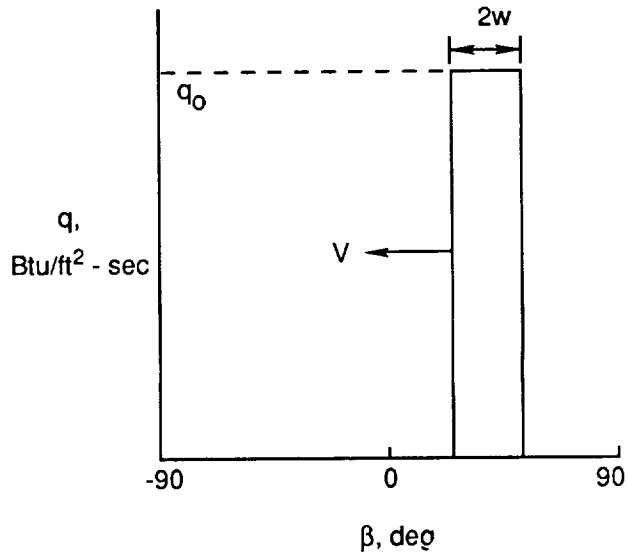

(b) Heating distribution assumed for transient case.

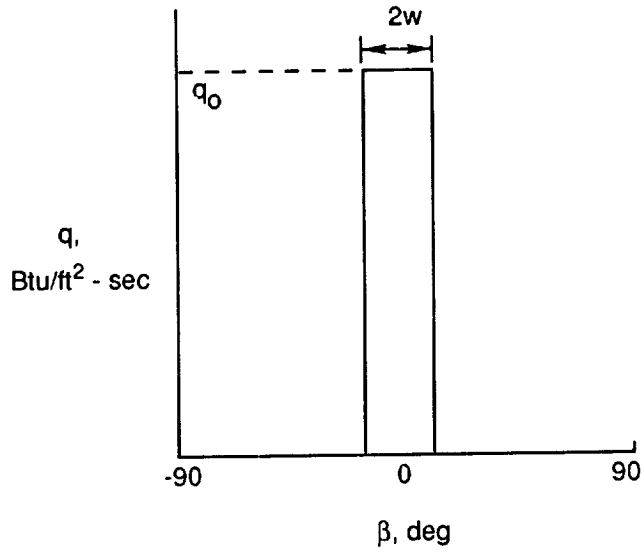

(c) Heating distribution assumed for steady-state case.

Figure 4. Type IV shock-wave-interference heating modeled as uniform square heat pulse for transient and steady-state cases.

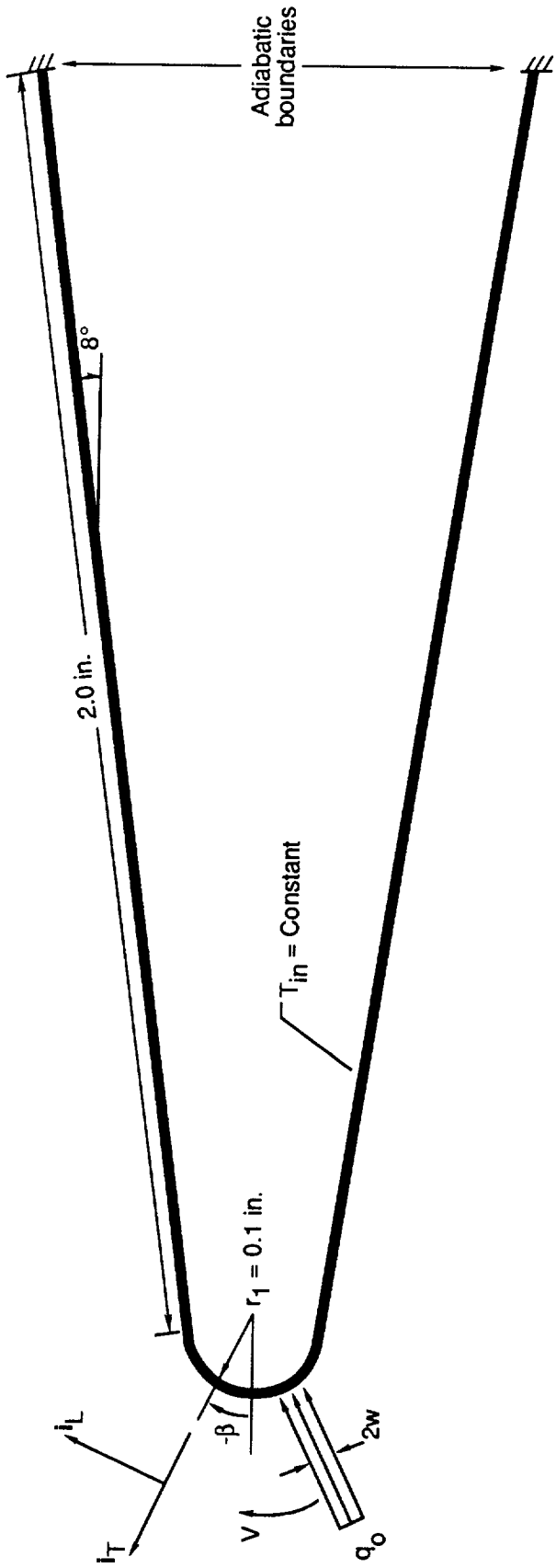

Figure 5. Baseline cowl-leading-edge geometry and coordinate system selected for study.

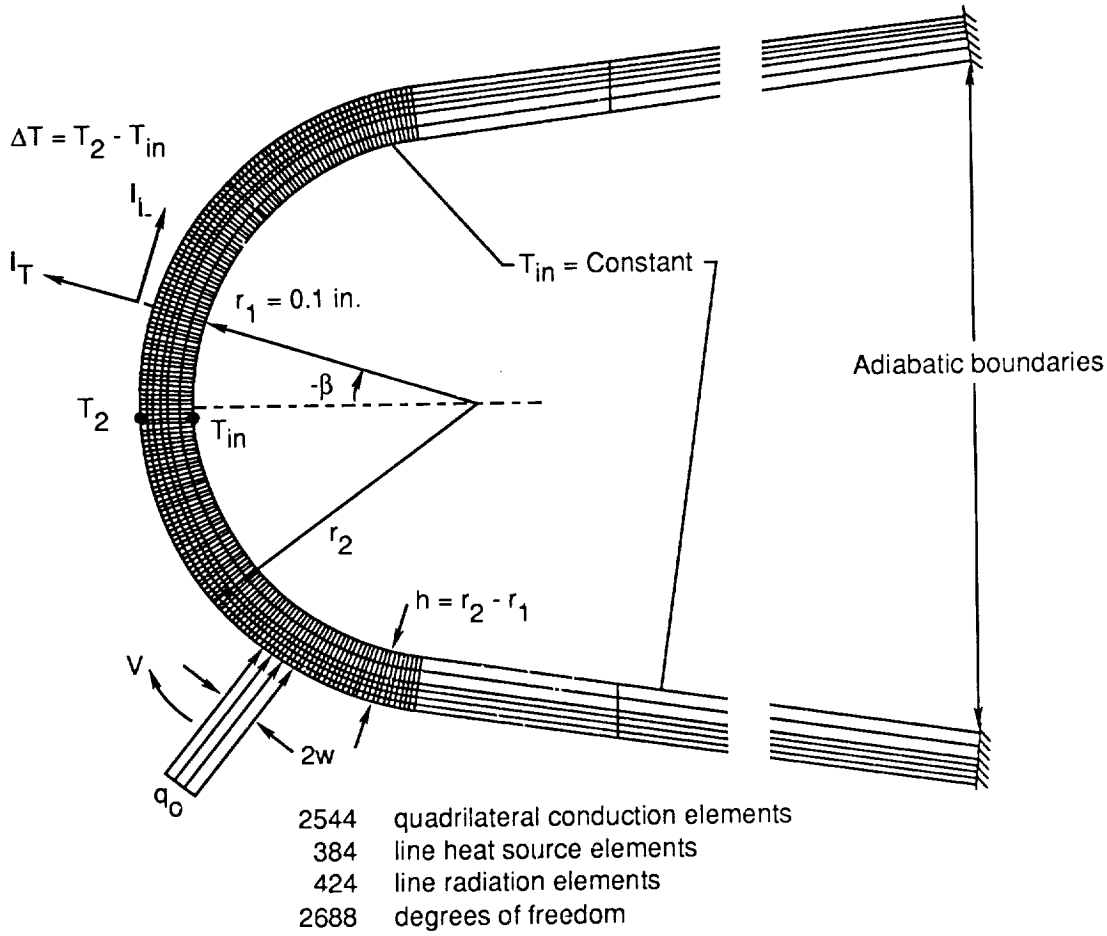

Figure 6. Detailed view of cylindrical portion of thermal-finite-element model of engine cowl leading edge.

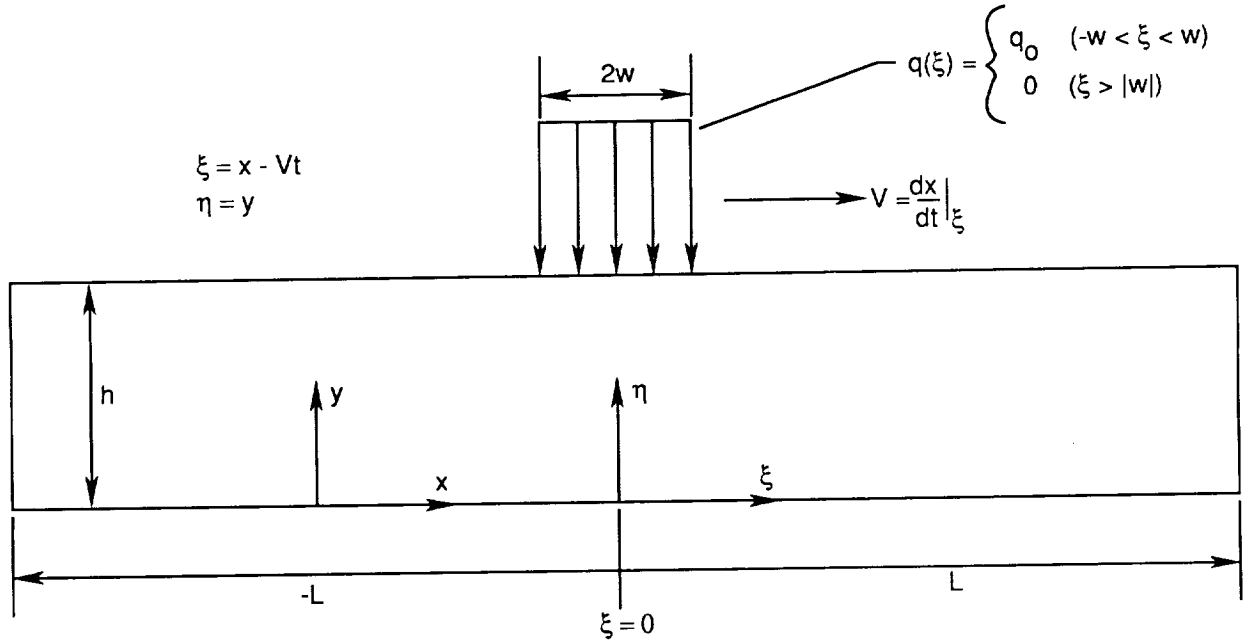

Figure 7. Approximate representation of Type IV shock-wave-interference heating for analytical solution.

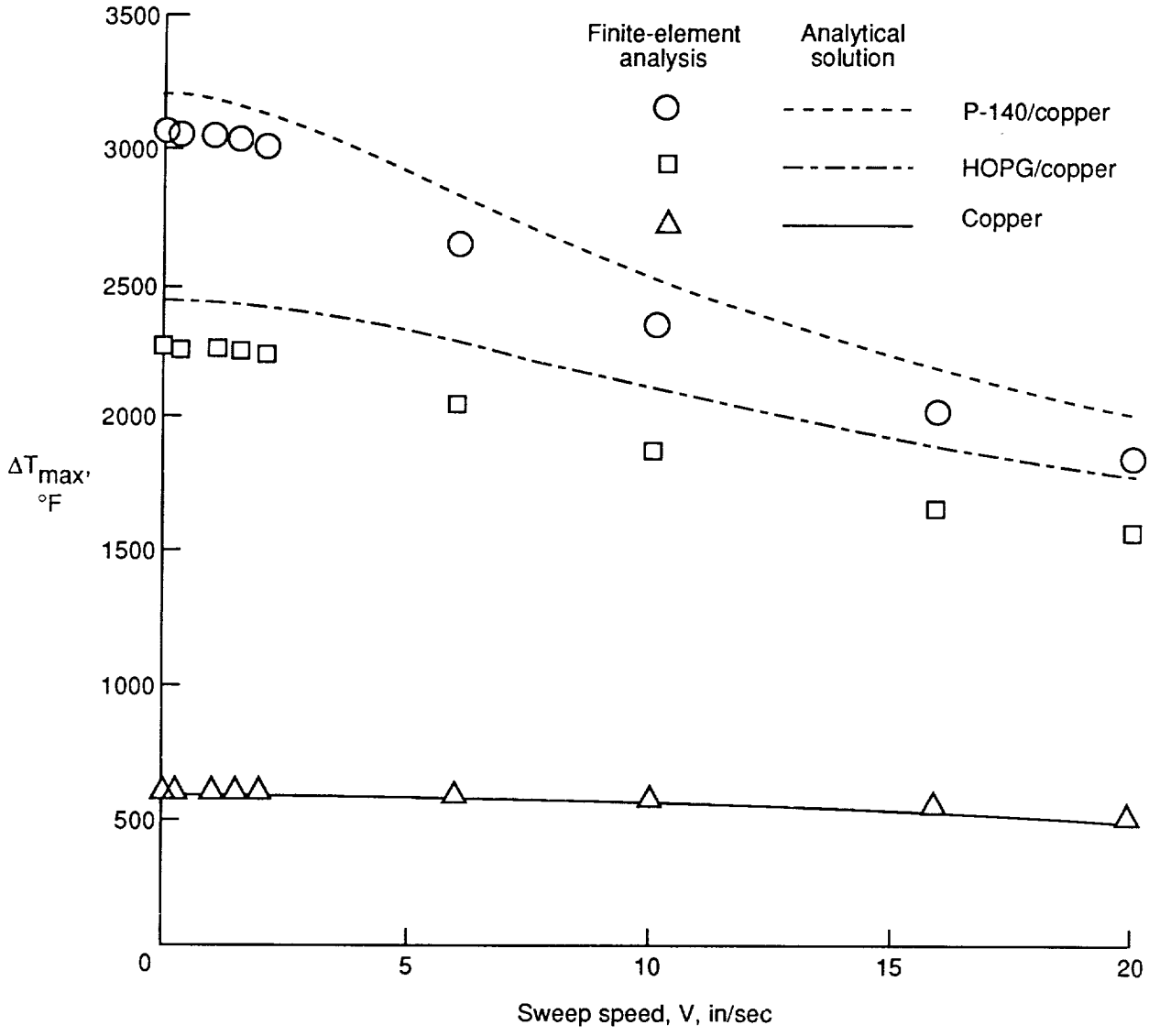

Figure 8. Effect of square-heat-pulse sweep speed on maximum temperature differences for copper and its composites. $h = 0.02$ in.; $2w = 0.01$ in.; $q_o = 50\,000$ Btu/ft^2-sec; $T_{in} = 0°$F.

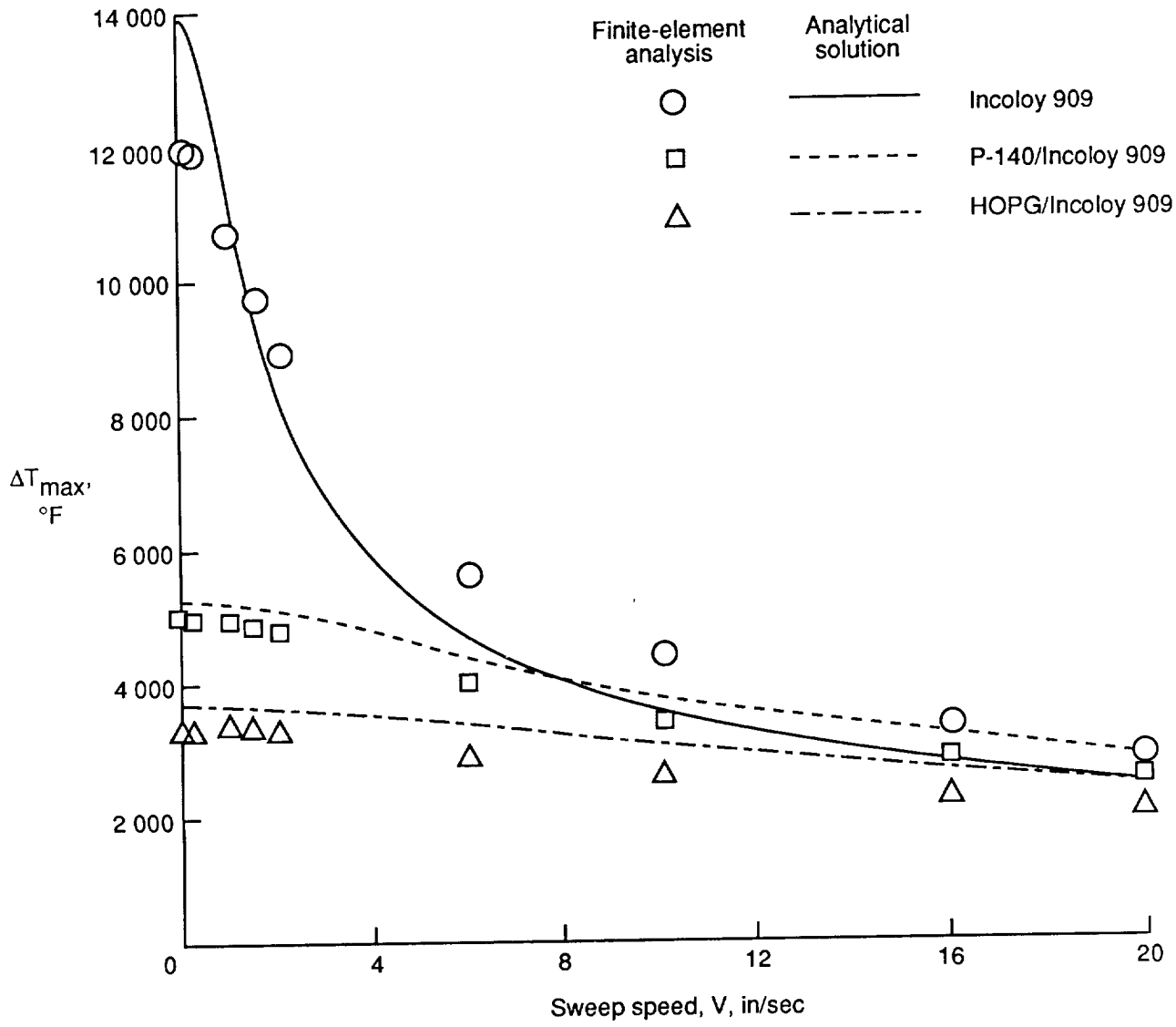

Figure 9. Effect of square-heat-pulse sweep speed on maximum temperature differences for Incoloy 909 and its composites. $h = 0.02$ in.; $2w = 0.01$ in.; $q_o = 50\,000$ Btu/ft^2-sec; $T_{\text{in}} = 0°\text{F}$.

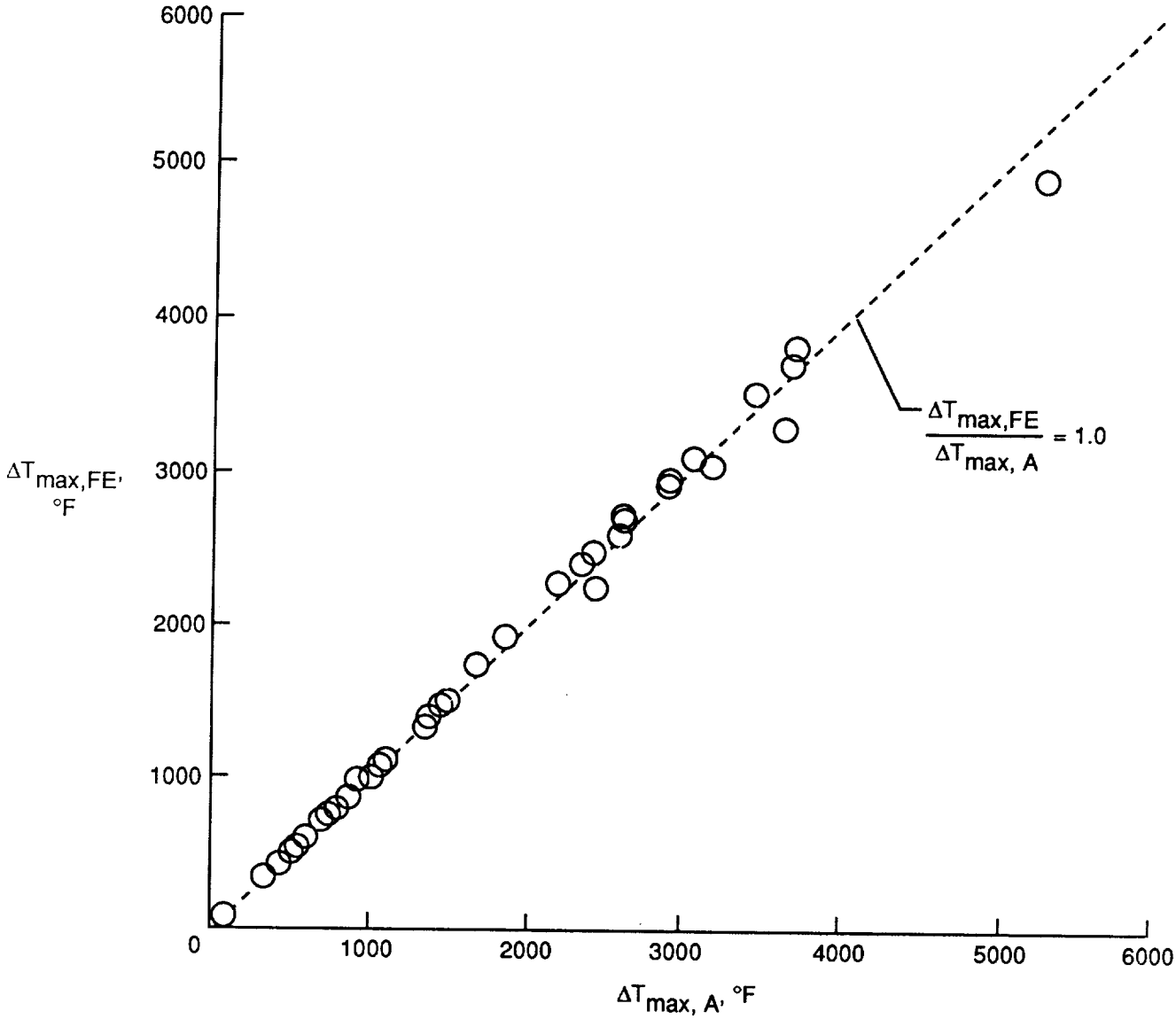

Figure 10. Comparison of finite-element and analytical-solution results for maximum temperature difference. $V = 0$ in/sec.

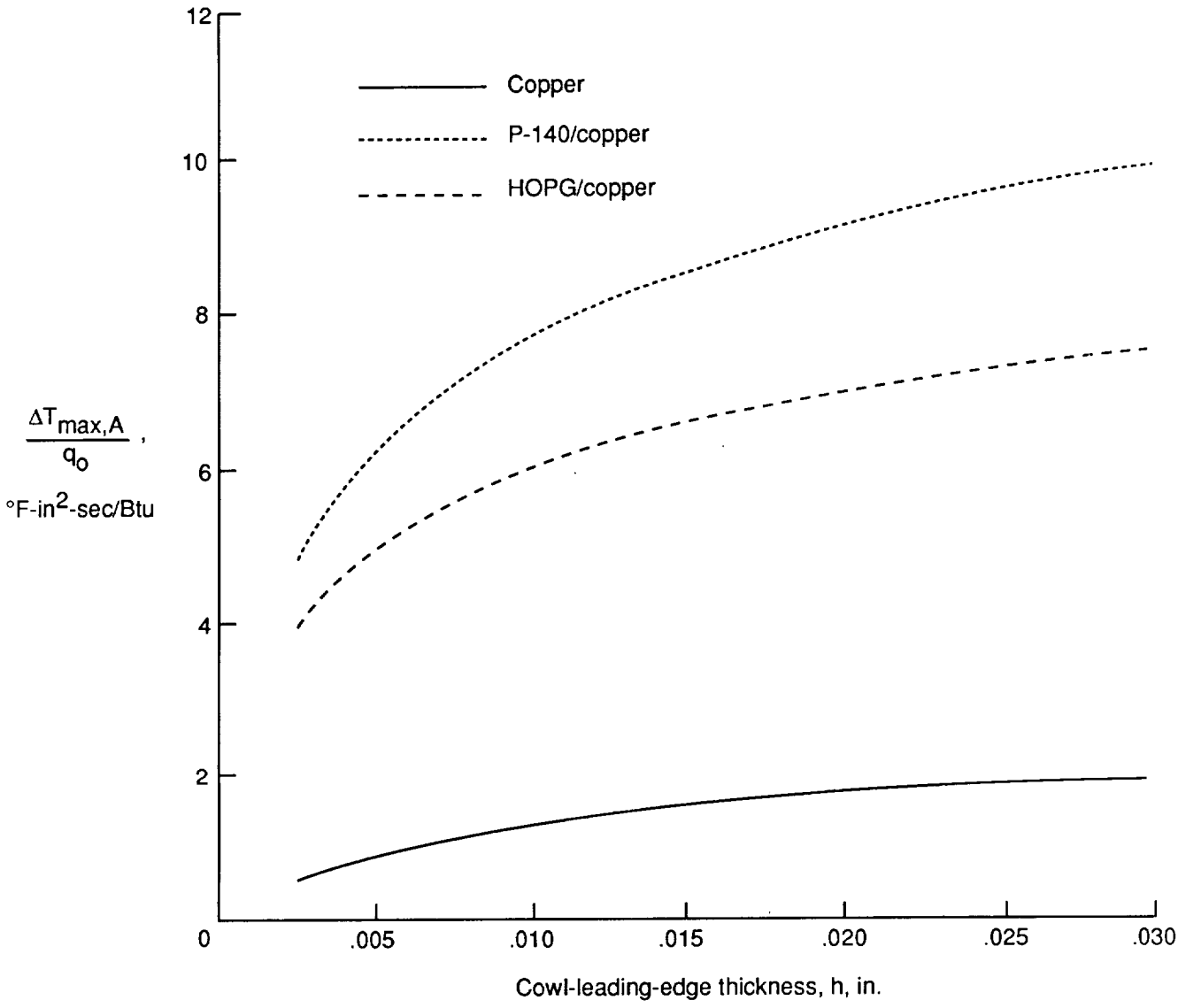

Figure 11. Effect of cowl-leading-edge thickness on maximum temperature difference for copper and its composites. $w = 0.005$ in.

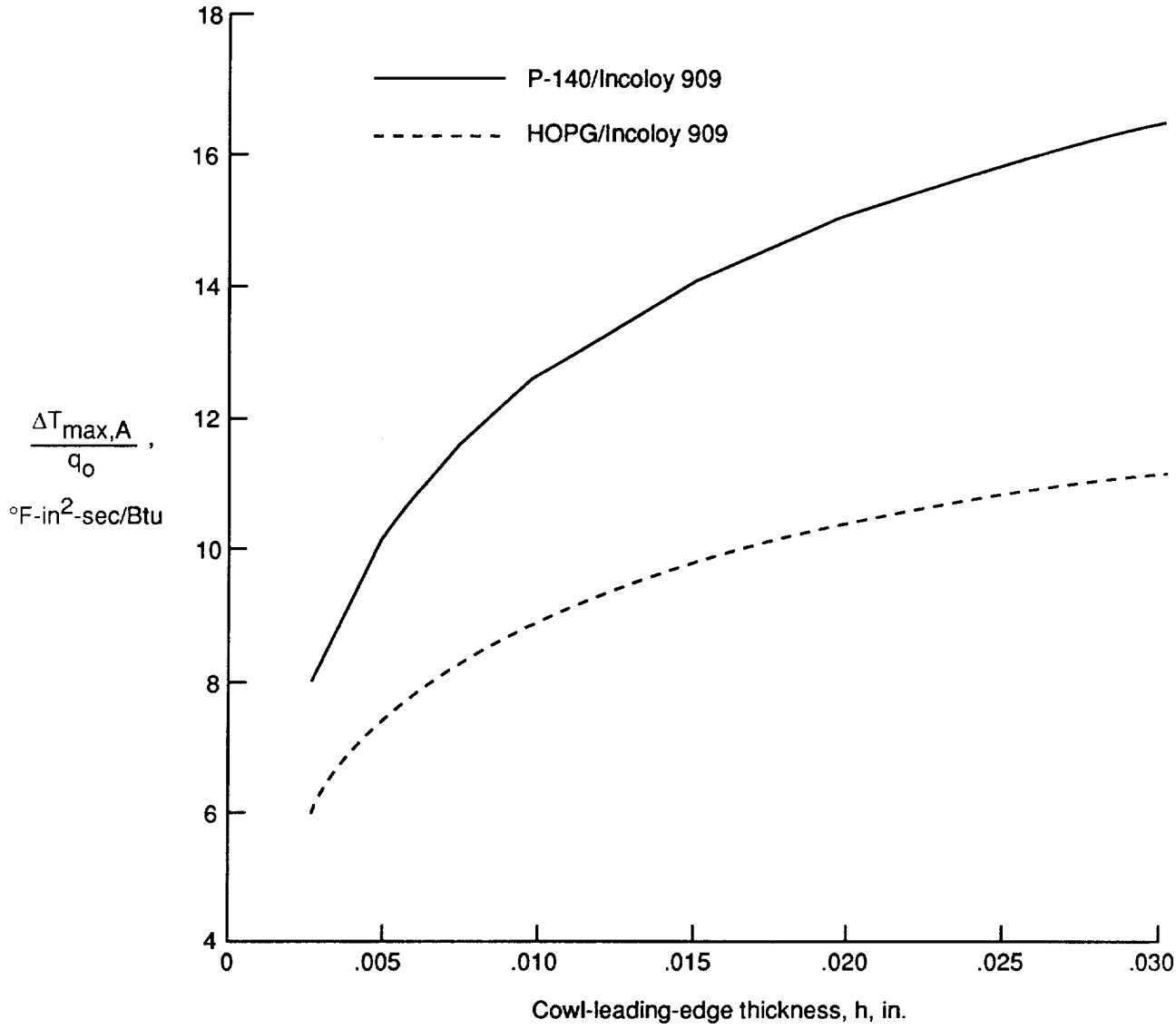

Figure 12. Effect of cowl-leading-edge thickness on maximum temperature difference for Incoloy 909 composites. $w = 0.005$ in.

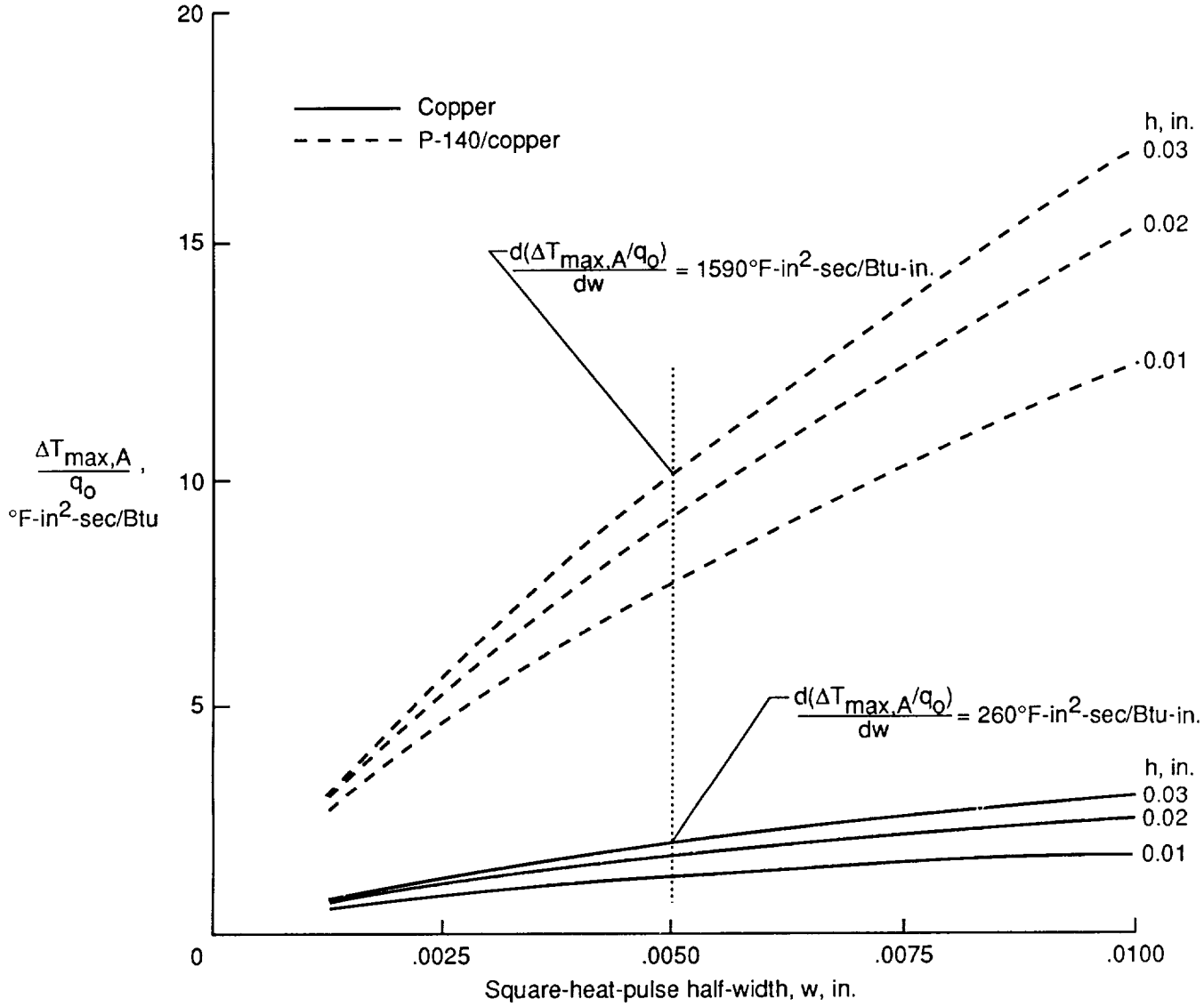

Figure 13. Effect of square-heat-pulse half-width on maximum temperature difference for copper and its composites.

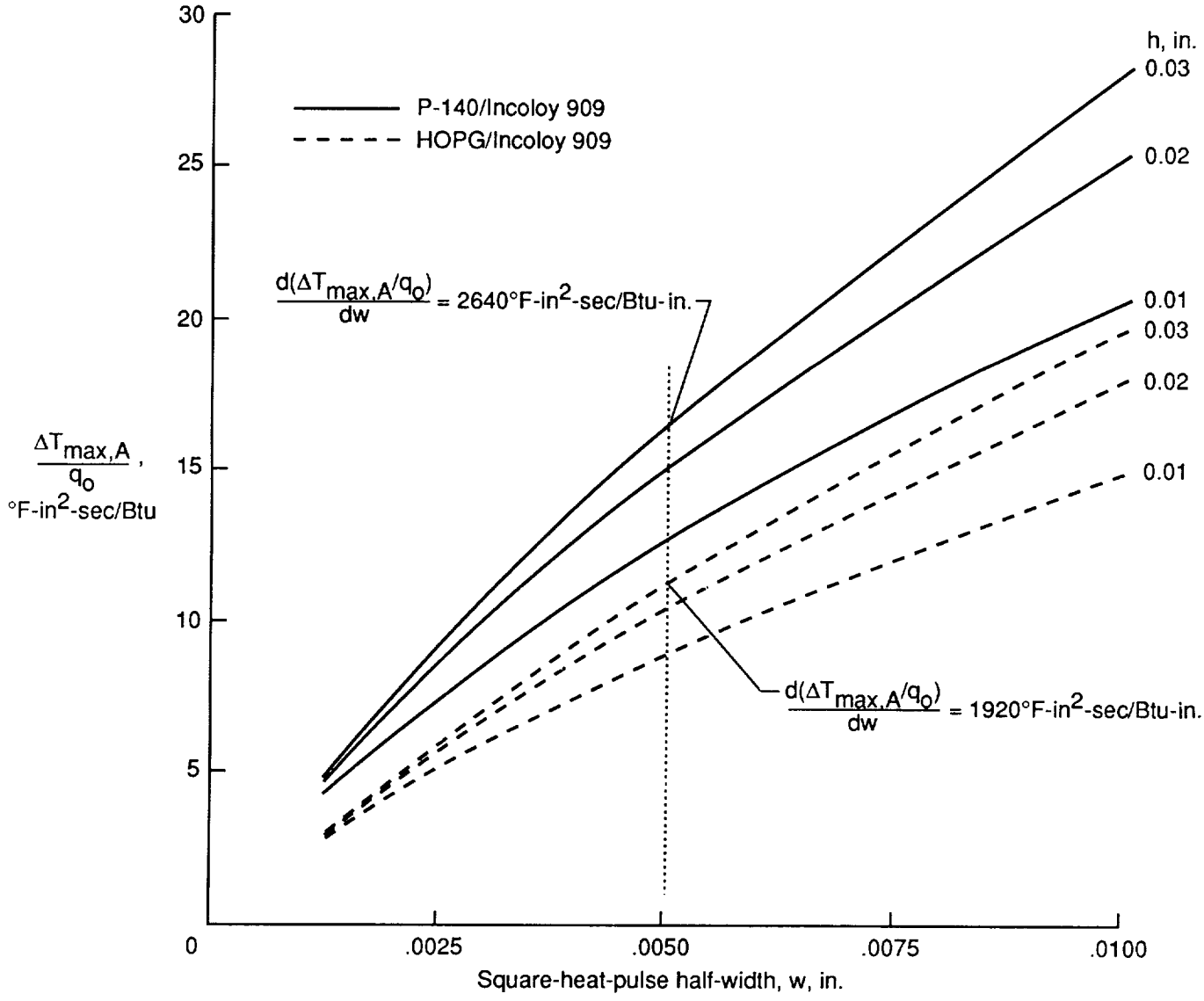

Figure 14. Effect of square-heat-pulse half-width on maximum temperature difference for Incoloy 909 composites.

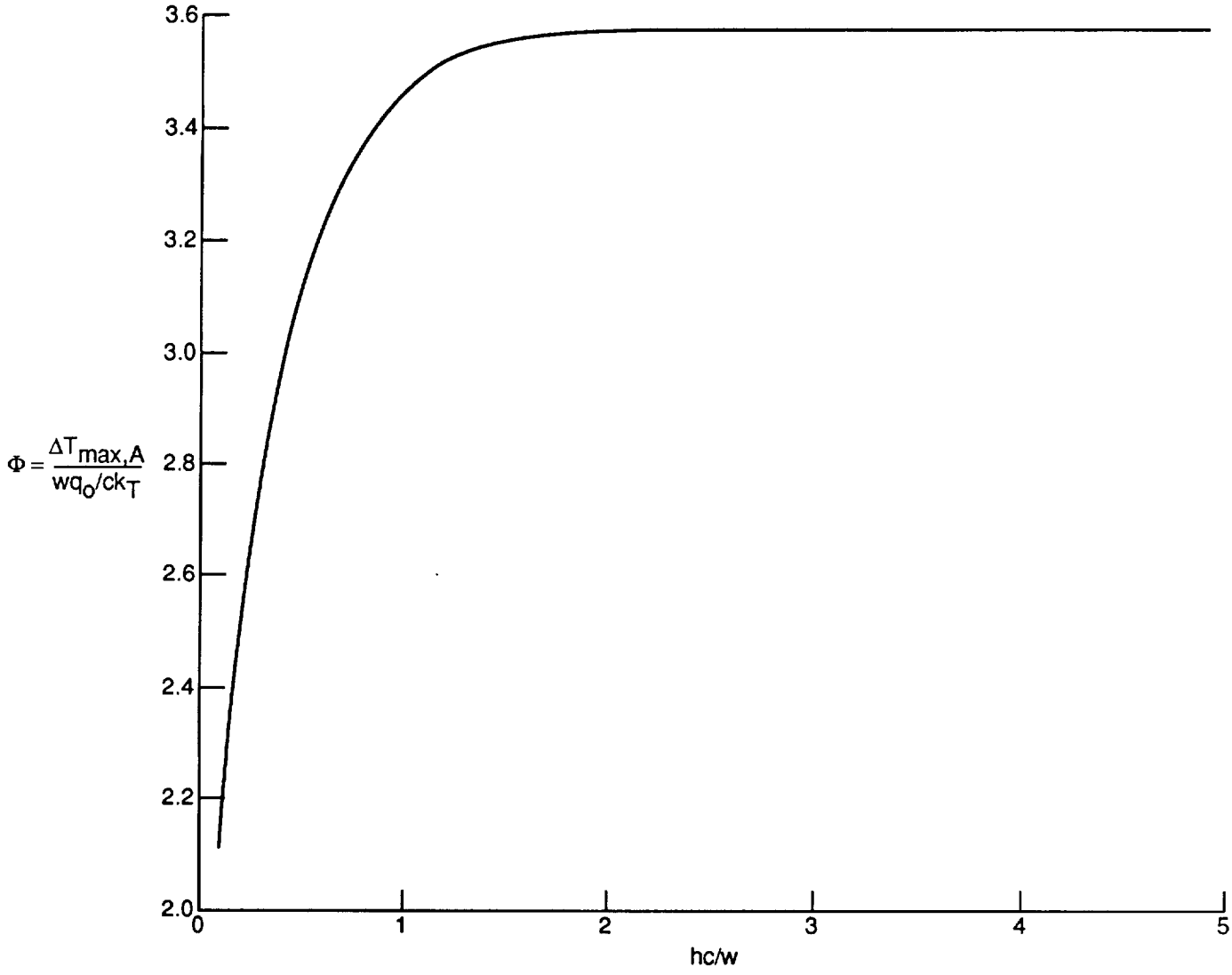

Figure 15. Nondimensional temperature difference as function of nondimensional length. $L/w = 80$.

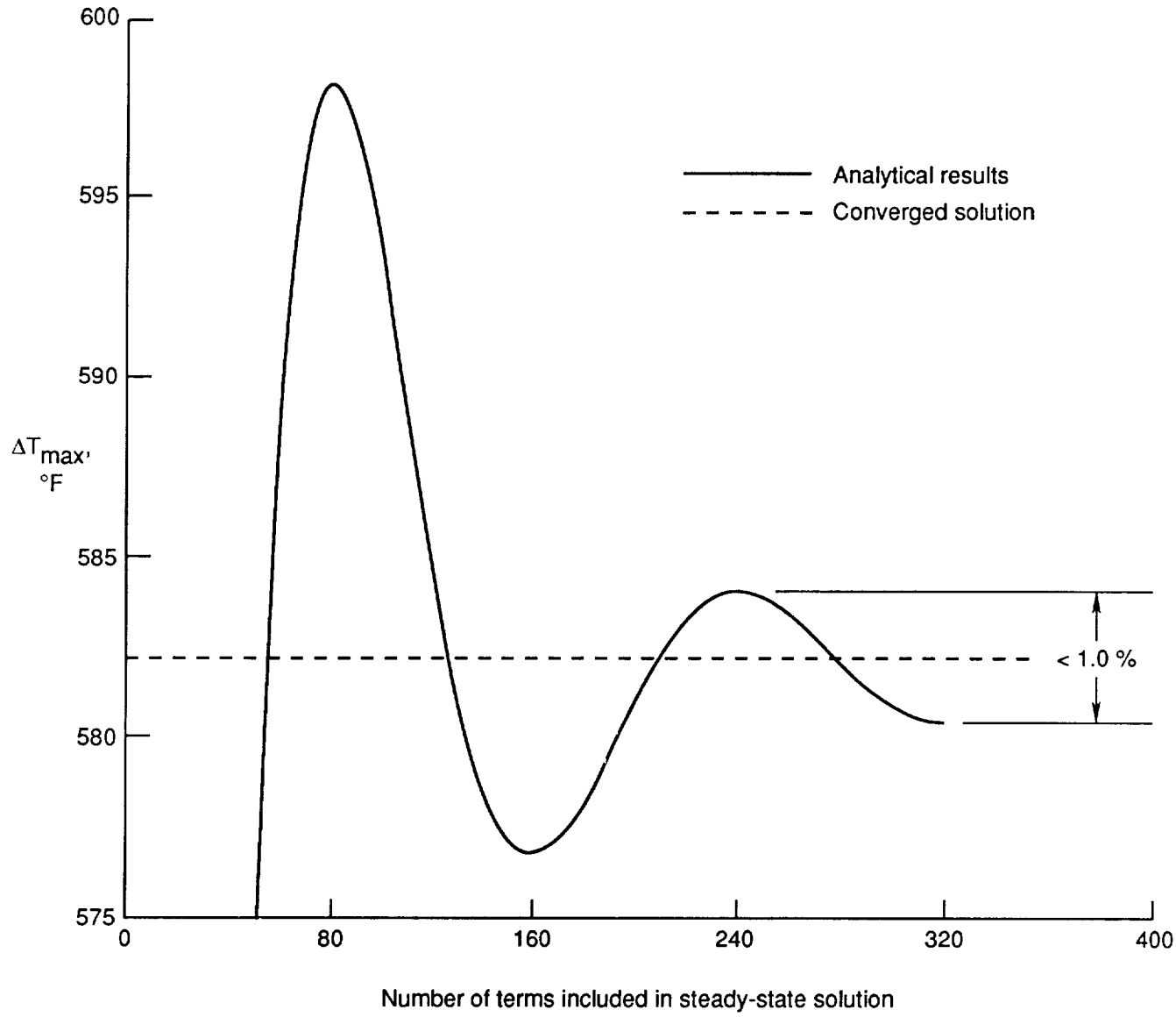

Figure 16. Maximum temperature difference as function of number of terms used in steady-state analytical solution.

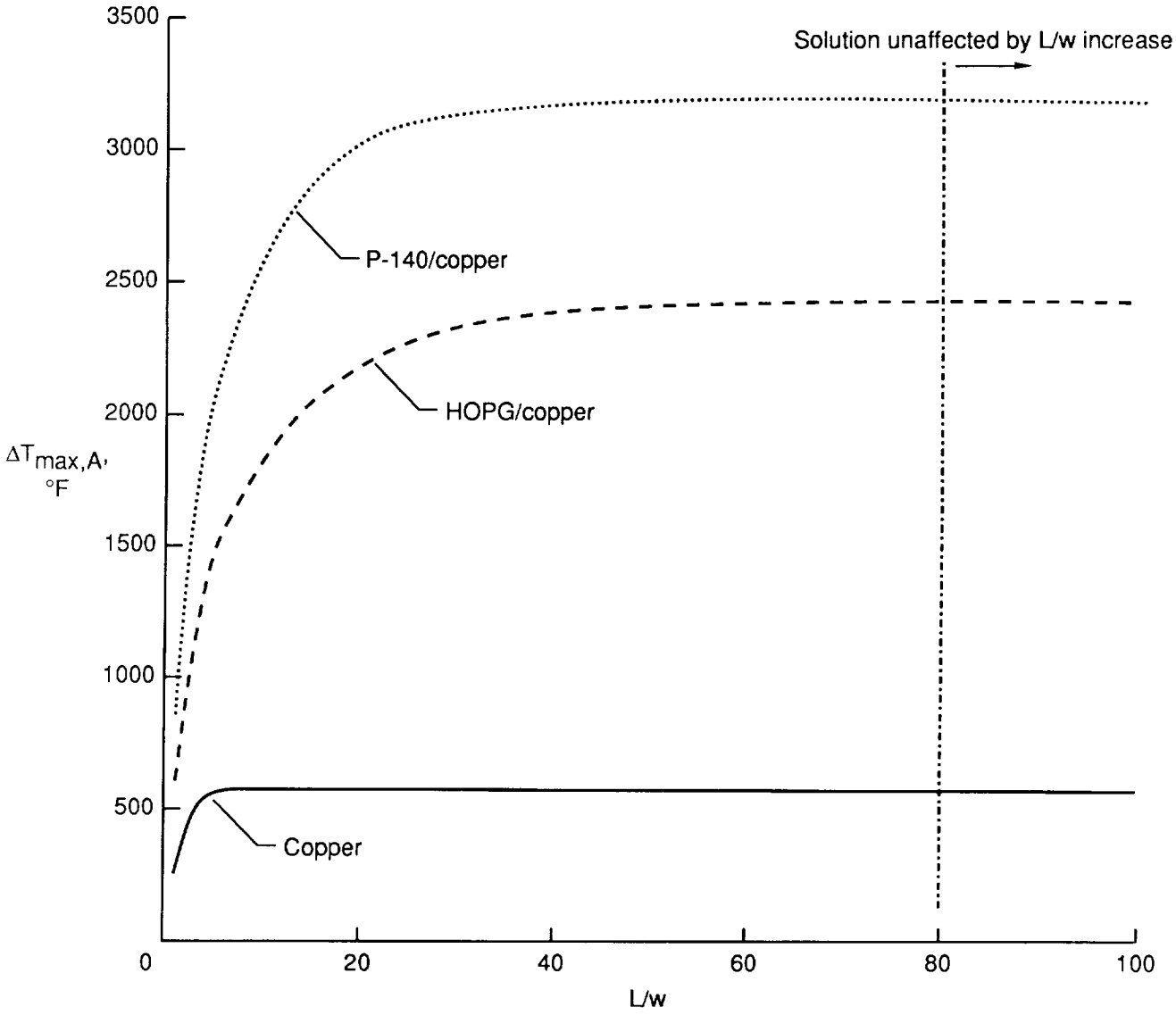

Figure 17. Effect of position of lateral boundary condition used in analytical solution on maximum temperature difference. $h = 0.02$ in.; $q_\circ = 50\,000$ Btu/ft^2-sec.

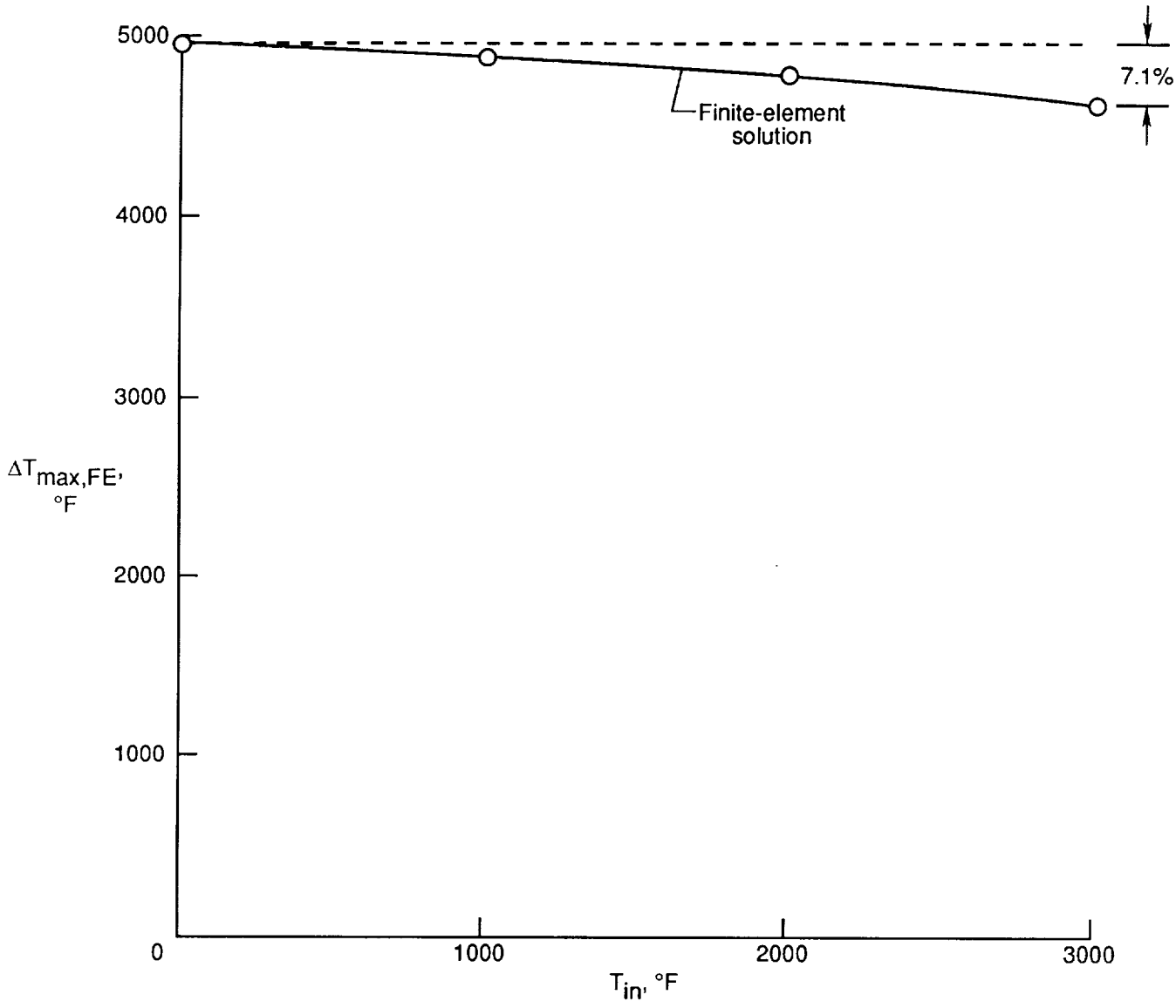

Figure 18. Effect of radiation on maximum temperature difference of P-140/Incoloy 909 composite as T_{in} is increased. k_L = 230 Btu/ft-hr-°F; k_T = 7 Btu/ft-hr-°F; h = 0.02 in.; w = 0.005 in.; q_o = 50 000 Btu/ft^2-sec.

REPORT DOCUMENTATION PAGE

Form Approved
OMB No. 0704-0188

1. AGENCY USE ONLY *(Leave blank)*	2. REPORT DATE	3. REPORT TYPE AND DATES COVERED
	March 1992	Technical Paper

4. TITLE AND SUBTITLE
A Simplified Method for Thermal Analysis of a Cowl Leading Edge Subject to Intense Local Shock-Wave-Interference Heating

5. FUNDING NUMBERS
WU 506-43-31-04

6. AUTHOR(S)
David M. McGowan, Charles J. Camarda, and Stephen J. Scotti

7. PERFORMING ORGANIZATION NAME(S) AND ADDRESS(ES)
NASA Langley Research Center
Hampton, VA 23665-5225

8. PERFORMING ORGANIZATION REPORT NUMBER
L-16505

9. SPONSORING/MONITORING AGENCY NAME(S) AND ADDRESS(ES)
National Aeronautics and Space Administration
Washington, DC 20546-0001

10. SPONSORING/MONITORING AGENCY REPORT NUMBER
NASA TP-3167

11. SUPPLEMENTARY NOTES

12a. DISTRIBUTION/AVAILABILITY STATEMENT
Unclassified Unlimited

Subject Category 34

12b. DISTRIBUTION CODE

13. ABSTRACT *(Maximum 200 words)*

Type IV shock-wave-interference heating on a blunt body causes extremely intense heating over a very localized region of the body. This paper presents an analytical solution to a heat-transfer problem that approximates the shock-wave-interference heating of an engine cowl leading edge of the National Aero-Space Plane. The problem uses a simplified geometry to represent the leading edge. An analytical solution is developed that provides a means for approximating maximum temperature differences between the outer- and inner-surface temperatures of the leading edge. The solution is computationally efficient and, as a result, is well suited for conceptual and preliminary design or trade studies. Transient and steady-state analyses are conducted, and results obtained from the analytical solution are compared with results of two-dimensional thermal-finite-element analyses over a wide range of design parameters. Isotropic materials as well as laminated composite materials are studied. Results of parametric studies are presented to indicate the effects of the thickness of the cowl leading edge and the width of the region heated by the shock-wave interference on the thermal response of the leading edge. Finally, a nondimensional temperature parameter is developed that is useful in evaluating the effects of several design parameters on the thermal response of the leading edge.

14. SUBJECT TERMS
Cowl leading edge; Parameter study; Shock-wave-interference heating; Moving-pulse heat load; Transient thermal analysis; Analytical solution ', HEAT AFFECTED ZONE

15. NUMBER OF PAGES
37

16. PRICE CODE
A03

17. SECURITY CLASSIFICATION OF REPORT	18. SECURITY CLASSIFICATION OF THIS PAGE	19. SECURITY CLASSIFICATION OF ABSTRACT	20. LIMITATION OF ABSTRACT
Unclassified	Unclassified		